Supramolecular Surface Chemistry

DOI: 10.1002/anie.200806339

Molecular and Supramolecular Networks on Surfaces: From Two-Dimensional Crystal Engineering to Reactivity

*Johannes A. A. W. Elemans, Shengbin Lei, and Steven De Feyter**

Keywords:
crystal engineering · chirality · nanostructures · scanning tunneling microscopy · supramolecular chemistry

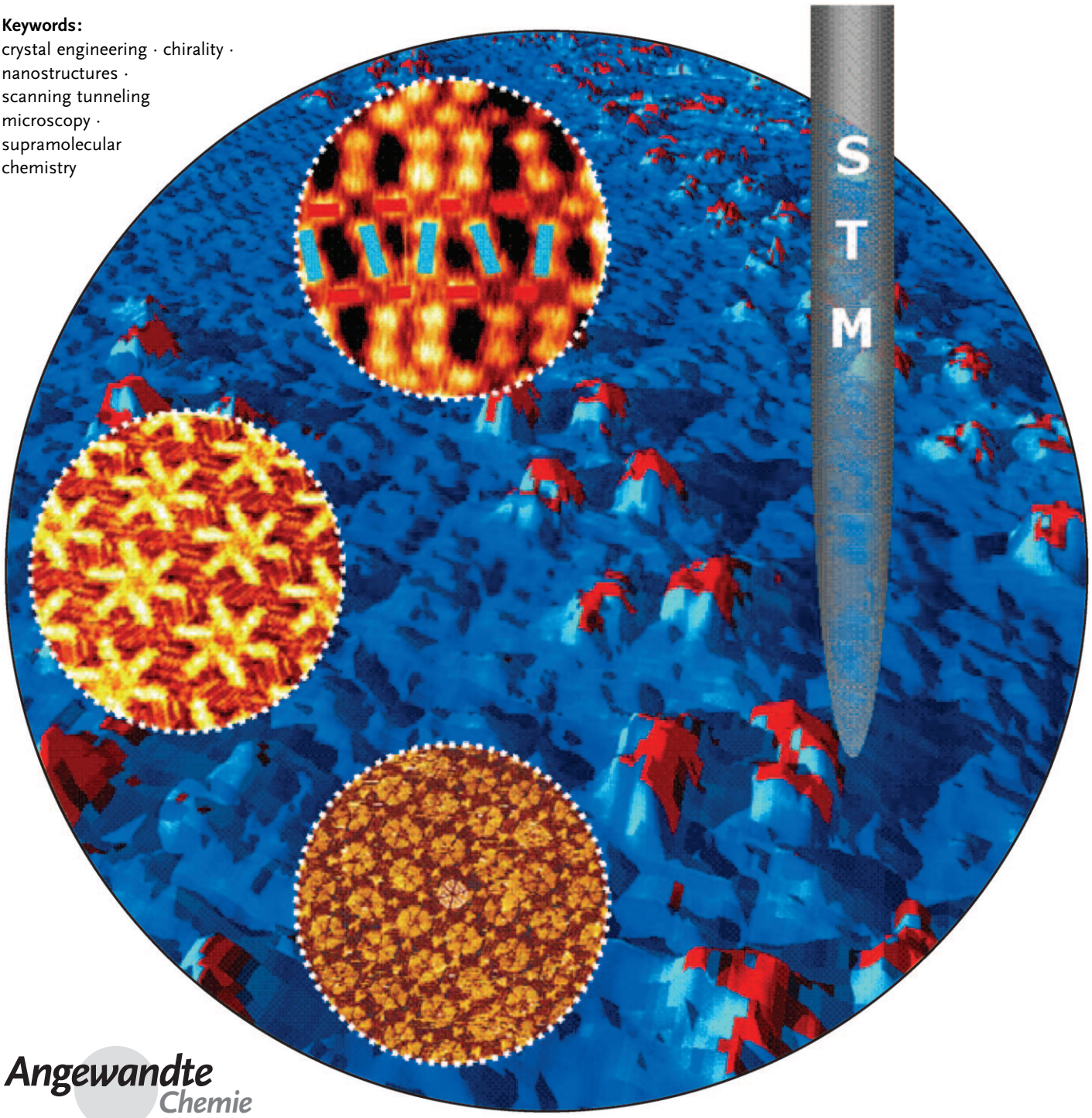

The invention of the scanning tunneling microscope has led to the visualization of molecules in real space on atomically flat conductive substrates. This has boosted research into supramolecular chemistry on surfaces. In this Review, we highlight recent developments in the design and functionality of supramolecular surface patterns, with special attention paid to those networks which are chiral or contain a high degree of porosity as well as to the reactivity, which is one of the most important recent developments in supramolecular surface chemistry.

From the Contents

1. Introduction 7299

2. Two-Dimensional Crystal Engineering on Surfaces: Dream or Reality? 7300

3. Chirality on Surfaces: Pasteur Would Love It ... 7305

4. Nanoporous Supramolecular Networks 7310

5. Chemical Reactivity on Surfaces: Along New Pathways 7322

6. Conclusions and Perspectives 7328

1. Introduction

In 1987, the Nobel Prize for Chemistry was awarded to Cram, Lehn, and Pedersen for exploring "chemistry beyond the chemical bond". Supramolecular chemistry, as it was called, deals with the way molecules interact with each other and how one can exploit noncovalent interactions to create higher order assemblies.[1] One of its important concepts is supramolecular self-assembly, which is described as "*the spontaneous association of either a few or many components resulting in the generation of either discrete oligomolecular supermolecules or of extended polymolecular assemblies such as molecular layers.*"[1] Most of the studies on supramolecular chemistry, particularly in the early stages, focused on solution-based systems, which revealed the fundamental concepts of this exciting field. A variety of structural and spectroscopic analysis techniques helped to unravel the (dynamic) structure of supramolecular assemblies and supermolecules. However, no visualization techniques in real space were then available to reveal details at the (sub)molecular level of these often complex architectures in the liquid phase.

In 1986, the Nobel Prize for Physics was awarded to Binnig and Rohrer for the invention of the scanning tunneling microscope, the first member of a class of instruments which are called scanning probe microscopes.[2] The common feature of these microscopes is that a sharp tip rasters a surface with high spatial resolution, even reaching the atomic scale. In this way, information about the topography and a variety of other surface properties can be obtained, depending on the particular features of the microscopy technique used. These new microscopes have boosted research in supramolecular chemistry and self-assembly on surfaces. Scanning tunneling microscopy (STM) in particular turned out to be extremely useful to probe not only the organization of molecules on a local scale, but also of molecular surface dynamics involved in the self-assembly process and the resulting electronic properties of the surface molecule.

Although initially not anticipated, the scanning tunneling microscope worked surprisingly well in a diverse range of environments, such as ultrahigh vacuum (UHV), at the liquid–solid interface and under ambient conditions. A metallic tip is brought very close to an atomically flat conductive substrate and a voltage is applied between both conductive media, which results in a tunneling current through a classically impenetrable barrier between the two electrodes. For imaging purposes, the tip and substrate are scanned precisely relative to one another and the tunneling current or tip–sample distance is accurately monitored as a function of the lateral position. The contrast in the STM images reflects both the topography and electronic effects.

The success and popularity of STM for the investigation of molecular self-assembly on atomically flat conductive surfaces is reflected in the steady increase in the number of papers published on self-assembly combined with STM—beginning with only a few papers in 1991 to about 200 publications in 2007 (according to the ISI Web of Knowledge).

The last decade has seen a steady increase in research devoted to the bottom-up construction of nanomaterials by the autonomous self-assembly of molecules on well-defined atomically flat surfaces, with the ultimate goal of creating functional nanosystems.[3] In this Review we highlight recent developments in the area of molecular self-assembly on surfaces, which mainly, but not exclusively, lead to two-dimensional crystalline monolayers, as revealed by STM. The structural aspects of self-assembly (two-dimensional crystal engineering) are highlighted, with special attention paid to surface chirality, nanoporous and multicomponent surfaces, and surface reactivity, which in our opinion are important current and future research themes. We deal exclusively with the self-assembly of molecular systems with a "large footprint", and do not treat, for example, self-assembled monolayers of alkyl thiols on gold.

[*] Dr. J. A. A. W. Elemans, Dr. S. Lei, Prof. S. De Feyter
Department of Chemistry, Division of Molecular and Nano Materials
and
INPAC—Institute for Nanoscale Physics and Chemistry
Katholieke Universiteit Leuven
Celestijnenlaan 200, 3001 Leuven (Belgium)
Fax: (+32) 16-327-990
E-mail: steven.defeyter@chem.kuleuven.be

2. Two-Dimensional Crystal Engineering on Surfaces: Dream or Reality?

2.1. Supramolecular Chemistry at a Surface

Just like in three dimensions, crystal engineering in two dimensions deals with elements of the well-known repertoire of noncovalent interactions that define supramolecular chemistry, such as hydrogen-bond-directed homo- and heteroassembly of molecules, dipole–dipole and van der Waals interactions, metal–ligand coordination, or a combination of several of them. The term "two-dimensional crystal engineering" is becoming increasingly recognized in recent years for surface-confined two-dimensional molecular aggregates.[4] Of the above-mentioned supramolecular interactions, hydrogen bonding and metal–ligand coordination are the most frequently encountered motifs that determine the self-assembly of molecules on a surface, because they are relatively strong and highly directional. Entropy effects should not be ignored though, as will be shown in the following sections. Furthermore, it is too simple to describe supramolecular self-assembly simply in terms of the change in free energy. Both at the liquid–solid interface and under UHV conditions, kinetic effects can overrule thermodynamically controlled self-assembly.

2.1.1. Hydrogen-Bonding Interactions

A series of benzenecarboxylic acids have proven to be excellent examples of "two-dimensional tectons" that form two-dimensional networks through hydrogen-bonding interactions. Phthalic acid, isophthalic acid (ISA), terephthalic acid (TA) and trimesic acid (TMA; Figure 1 a) all contain carboxylic acid groups that are at the same time strongly directional hydrogen-bond donors and acceptors. Phthalic acid does not form monolayers at a liquid–solid interface, because of steric hindrance between the adjacent carboxylic acid groups of the molecule preventing it from being planar. It would, furthermore, be conceptually impossible for this molecule to form extended arrays based upon hydrogen bonding. In contrast, ISA and TA form densely packed monolayers in which the molecular organization is dominated by hydrogen-bonding interactions.[5] Encoded by its substitution patterns, TA self-assembles into linear arrays, while ISA is organized in a zigzag fashion (Figure 1 b,c). TMA, which has an additional carboxylic acid functionality, forms (amongst other polymorphs) a honeycomb network of fused

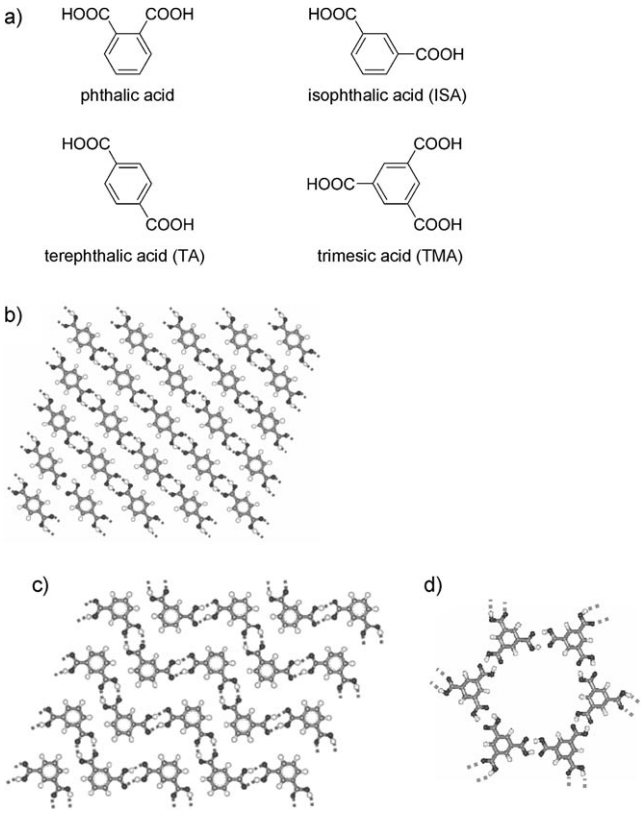

Figure 1. a) Molecular structures of different benzenecarboxylic acids; observed arrangement of b) TA; c) ISA, and d) TMA in a two-dimensional crystal at the surface. Reprinted from Ref. [5] with permission from the American Chemical Society.

Hans Elemans completed his PhD in physical organic chemistry in 2001 with Prof. Roeland J. M. Nolte at the Radboud University Nijmegen (The Netherlands). Since 2003, he has occupied a bridging position between the solid-state physics and organic chemistry groups working in the field of reactivity at surfaces. He was awarded Veni and Vidi innovative research grants in 2004 and 2008 for his work. In 2008 he worked in the group of Prof. Steven De Feyter at K. U. Leuven (Belgium).

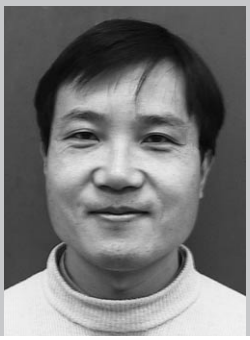

Shengbin Lei obtained his PhD in 2002 in physical chemistry at the Institute of Chemistry, CAS (China) with Prof. Chen Wang. Thereafter he worked first as an assistant and then associate professor at the same institute, working on surface assembly and scanning tunneling microscopy. In 2006, he joined the group of Prof. Steven De Feyter at K. U. Leuven, where he works on two-dimensional nanoporous networks and host–guest chemistry.

Steven De Feyter is professor at K. U. Leuven in Belgium. After starting up scanning tunneling microscopy during his PhD at K. U. Leuven, he moved for a postdoctoral position to the group of Prof. Ahmed Zewail (California Institute of Technology, Pasadena). His current interests include the study of supramolecular chemistry and self-assembly phenomena at surfaces with scanning probe methods with a focus on solid–liquid interfaces.

cyclic hexamer arrays (Figure 1d).[6] The well-defined and robust pores in these arrays provide the exciting potential to host small guest molecules, which can be incorporated into the network in a repetitive and spatially ordered arrangement.[7] TMA networks have been applied as hosts for a variety of guests such as fullerenes[8] and coronenes (see Section 4).[9] Furthermore, these two-dimensional TMA tectons form the basis for a variety of (multicomponent) surface architectures.[10]

Although two-dimensional crystalline phases are often formed, this is not always the case, as illustrated by the self-assembly of *p*-terphenyl-3,5,3′,5′-tetracarboxylic acid (TPTC; Figure 2a) at the interface of graphite and 1-nonanoic acid.[11] The carboxylic acid groups can stabilize two assembly motifs,

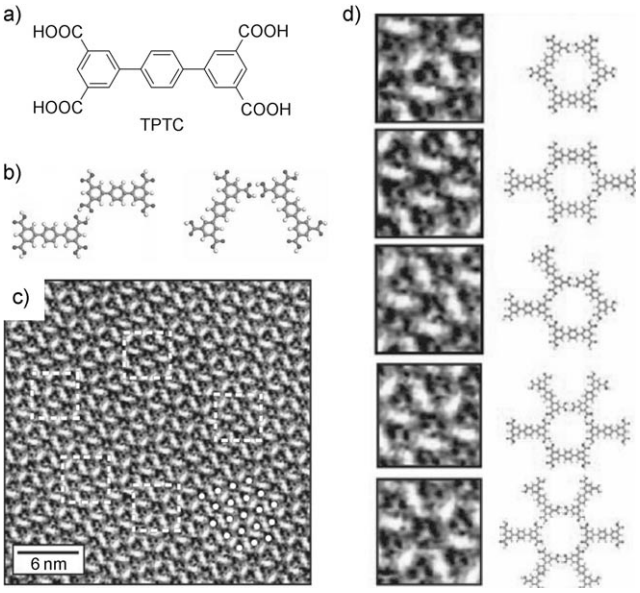

Figure 2. a) Molecular structure of TPTC; b) two possible assembly motifs of TPTC at the liquid–solid interface: parallel (left) and in the form of an arrowhead (right); c) STM image of the TPTC network at the graphite–1-nonanoic acid interface; the dashed squares indicate the five possible tilings enclosing a pore, and the dots indicate the hexagonal lattice of the pores; d) magnification of the five possible tiling arrangements (left) and the corresponding molecular models (right). Reprinted from Ref. [11] with permission from the American Association for the Advancement of Science.

namely the "parallel" and "arrowhead" configurations shown in Figure 2b, by means of hydrogen-bonding interactions. The network at the liquid–solid interface, as revealed by STM, consists of a highly regular hexagonal pattern of pores, separated by walls of TPTC molecules (Figure 2c). Interestingly, the number and arrangement of the TPTC molecules around the pores is random, and consists of one of the five possible tilings shown in Figure 2d. As a result, the network exhibits orientational symmetry (the pores are at fixed distances), but lacks translational order. Theoretical calculations revealed that after formation of the network the tiles are trapped in a large number of local minima of a complex energy landscape, similar to that observed in a three-dimensional glass, thereby giving rise to entropically stabilized randomness in the rhombohedral pattern. The only rearrangements that were observed experimentally occur sporadically around triangular topological defects that propagate through the network and involve the movement of one TPTC molecule at a time.

2.1.2. *Metal–Ligand Coordination*

Although of a different nature, metal–ligand coordination interactions share the same properties as hydrogen-bonding interactions as far as specificity and directionality are concerned. The rich coordination properties of transition metals with organic ligands, in terms of stoichiometry as well as the angle, strength, and reversibility of binding, has inspired the construction of a range of well-defined two-dimensional surface aggregates, the structure of which can in many cases be predicted from recently established design rules, at least for some of the well-established bonding schemes. However, the presence of a surface results in clear differences having been observed when metal–ligand interactions in three or two dimensions are compared, for example, deviating binding stoichiometries or angles.

Some two dimensional metal–ligand coordination aggregates, such as coordination polymers[12] or grids[13] have been imaged under ambient conditions, but the majority of them have been constructed under UHV conditions where chemically labile metal–ligand complexes can more easily survive. The research group of Kern in particular has developed a wealth of metal–ligand networks simply by evaporating well-defined stoichiometries of the components onto surfaces. In some cases metal atoms were not evaporated but directly "extracted" from the underlying surface and included in between the ligands.

Recently, such metal–ligand networks were very elegantly applied in an STM study dealing with some of the key factors of self-assembly (self-recognition, self-selection, self-repair, and dynamic reorganization).[14] A library of linear polyaromatic dicarboxylic acids, bipyridines, and Fe atoms were used as building blocks. By using this combination, carboxyl and pyridine ligands coordinate to dimers of Fe centers in the highly specific geometry shown in Figure 3a. When the components of the library were co-deposited together with Fe atoms on a Cu(100) surface in a UHV scanning tunneling microscope, highly regular porous networks were obtained in which the "horizontal rows" consist of the dicarboxylate ligands and the "vertical pillars" are formed by the bipyridine ligands (Figure 3b). However, a distorted network was obtained when a ternary combination of one bipyridine and two carboxylic acids was deposited, thus indicating the low level of structural organization achieved; this organization did not improve upon annealing the surface (Figure 3c). The weakly binding bipyridine pillars simply adapt themselves, by tilting their angles, to the random sequence of strongly interacting arrays of Fe centers and dicarboxylates. This error tolerance and the failure of the system to reach thermodynamic equilibrium by phase separating the networks is caused by the high stability of the iron–carboxylate coordination bonds compared to the rather labile axial iron–pyridine interactions and dictates the final arrangement of the

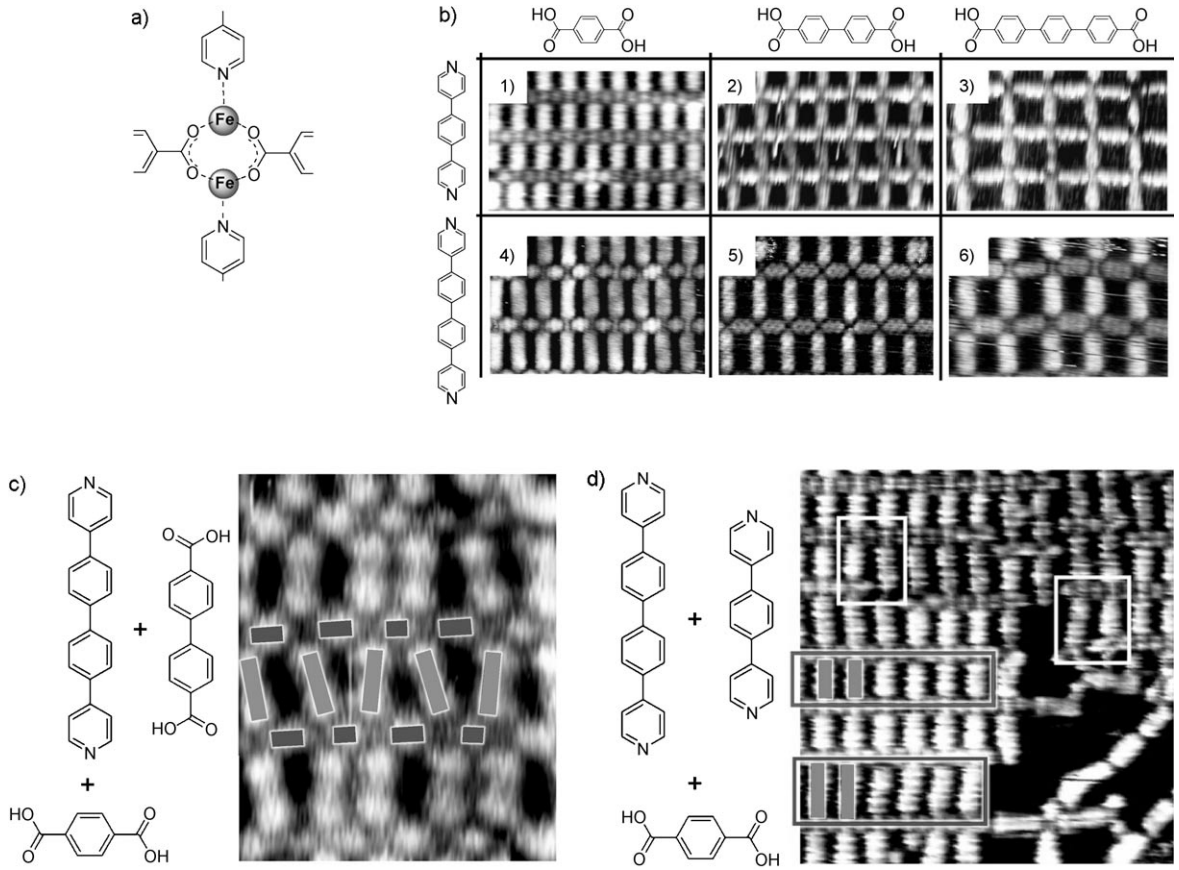

Figure 3. a) Coordination motif in networks composed of Fe centers and pyridine and carboxylic acid ligands; b) UHV STM images (all 9.4×6.0 nm^2) of networks formed by the coassembly of Fe centers with six possible combinations of bipyridine and dicarboxylic acid ligands (1–6); c) UHV STM image (6.0×9.6 nm^2) of a distorted network formed by Fe centers and a ternary mixture of one bipyridine and two different dicarboxylic acid ligands; d) STM image (14×14 nm^2) of a network formed by Fe centers and a ternary mixture of one dicarboxylic acid and two different bipyridine ligands under UHV conditions; white boxes: defects; dark boxes: highly ordered subdomains. Reprinted from Ref. [14] with permission from the National Academy of Sciences, USA.

components within the metastable structure. In contrast, significant self-repair was observed when a mixture of two bipyridine ligands and one dicarboxylic acid was used (Figure 3d). In this case, local phase separation does occur and separate subdomains are formed with bipyridine ligands of uniform length; this finding implies the occurrence of self-selection and self-recognition. Of critical importance to these processes is the possibility of self-repair, which in this mixture relies on a reversible coordination of the bipyridine ligands.

2.1.3. *Other Types of Interactions*

Less predictable supramolecular interactions (such as dipole–dipole and van der Waals interactions) between molecules are generally weaker than hydrogen bonding and metal–ligand interactions, but they can still play a decisive role in self-assembly processes at a surface, in particular when they operate cooperatively. Electrostatic interactions between molecules adsorbed at a surface can lead to highly ordered patterns, while the closest atoms of nearest neighbor molecules are well-separated. A typical example of such behavior is the formation of honeycomb patterns of polar subphthalocyanines at a Ag(111) surface, where the physisorbed molecules are separated by about three lattice spacings of the substrate (Figure 4).[15] A delicate balance between molecule–substrate and molecule–molecule interactions, in combination with the local polarizability of the underlying substrate, govern the specific formation of such patterns. These patterns can become even more complex when polarizable molecules such as fullerenes are included as a second component.[16]

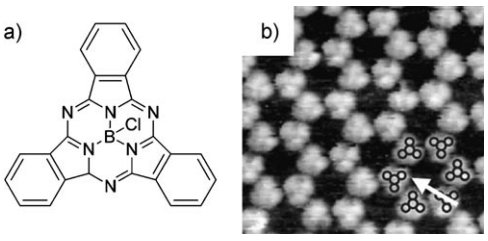

Figure 4. a) Molecular structure of the subphthalocyanine; b) UHV-STM image (14×14 nm^2) of a honeycomb pattern of the molecule on Ag(111); the arrow indicates one of the phenyl rings. Reprinted from Ref. [15] with permission from the American Physical Society.

Interdigitation of alkyl chains is a frequently encountered stabilization motif within self-assembled monolayers of organic molecules, particularly at liquid–solid interfaces. This stabilization occurs not only by means of interactions between the chains in a lattice, but also by van der Waals interactions with the surface running parallel to them. Graphite surfaces in particular have a high affinity for alkyl chains, because of the high degree of structural matching, and the molecule–substrate interactions can generally be controlled by varying the chain length.

2.2. Role of the Substrate and the Medium

Many of the supramolecular interactions that exist in three dimensions can be translated to self-assembled structures built in two dimensions. However, two-dimensional self-assembly is complicated by two additional factors that require special attention: the role of the substrate, and the role of the medium from which molecules are adsorbed onto that substrate.

When molecules are to be organized into well-defined two-dimensional patterns it is no surprise that the nature of the underlying substrate is of essential importance. It is almost never an innocent factor, since it can strongly direct the self-assembly process by guiding the organization of molecules into epitaxial layers, even when only weak interactions are present between the adsorbed molecules and the substrate. Detailed experimental and theoretical studies have revealed that the tendency of molecules in a two-dimensional monolayer to comply with the local registry of a close-packed surface can result in significant changes in intermolecular interactions when compared to their self-assembly in three-dimensional crystals. Klappenberger et al. addressed this behavior when they compared the self-assembly of *N*,*N*-diphenyloxalamide in the bulk crystal with that in a monolayer of the compound on a Ag(111) surface under UHV conditions.[17] While the molecules are organized in arrays stabilized by a multitude of intermolecular hydrogen-bonding interactions in the crystal structure, their confinement on the surface results in a totally different intermolecular binding motif. One-molecule-thick linear chains consisting of supramolecular polymers of the compound are formed, in which only one intermolecular hydrogen-bonding interaction remains (Figure 5). In addition, the phenyl rings are rotated away from their favorable geometry (flat on the surface) to allow the molecules to get close enough to establish this hydrogen-bonding interaction.

This means that a surface can be considered an extra complicating factor in addition to the supramolecular chemistry processes in solution, but this can also be used to an advantage since the difference between substrates can be used to fine-tune two-dimensional self-assembly through templating effects. Ideally, such a substrate should be flat over large domains and free of defects. A wide range of atomically flat metal surfaces is available under UHV conditions, but many of these are not stable under ambient conditions or upon exposure to a liquid. In those cases, a more inert material is desired, such as highly oriented pyrolytic graphite (HOPG), which has been the favorite substrate of choice for numerous STM studies on physisorbed monolayers of organic molecules. Other popular substrates for use under ambient conditions are Au(111), MoS_2, and $MoSe_2$.[18] Although an epitaxial relationship with the underlying substrate is observed for the majority of organic monolayers, some examples are known of molecular self-assembly where less or no registry is present between the supramolecular adlayer and the substrate. Recent examples involve the self-assembly of dye molecules on insulating surfaces, which is of interest for the development of molecular electronics devices, since in that case the substrate can act as an insulator for electronically interacting molecules.[19] Ramoino et al. were the first to image extended ordered monolayers of copper octaethyl porphyrins on 1–3 monolayer thick islands of NaCl on metal surfaces under UHV conditions.[20] The adsorption of the molecules occurs in a hierarchical fashion: upon increasing the monolayer coverage, ordered and still epitaxial porphyrin arrays are first formed on the metal substrate, followed by assembly on the first and then second monolayer of NaCl. This stepwise assembly process was explained by a rapid decrease in the strength of the van der Waals interaction between the molecules and the substrate as the number of insulator layers increased. More recent research described the complete loss of epitaxy when porphyrin molecules were self-assembled on a bulk isolator crystal and visualized with the help of high-resolution noncontact atomic force microscopy (nc-AFM).[21] *meso*-(4-Cyanophenyl)-functionalized zinc porphyrins evaporated on KBr(001) were found to self-assemble in an "edge-on" fashion in monolayers of parallel molecular wires along the [110] direction of the substrate (Figure 6). Although the cyano groups point downwards in these wires to interact with the KBr surface through electrostatic interactions, the molecule–molecule separation does not match with the repeating distances in the ionic lattice underneath (Figure 6b).

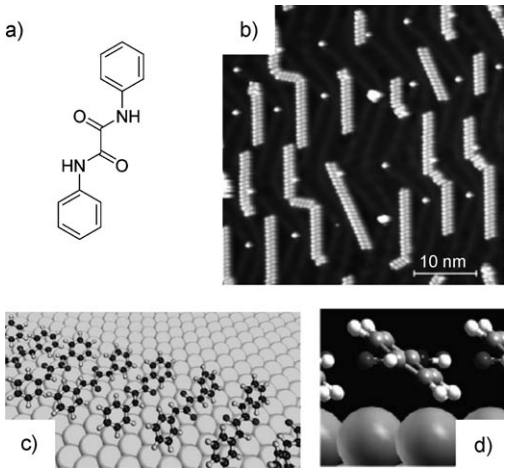

Figure 5. a) Molecular structure of *N*,*N*-diphenyloxamide; b) STM image of one-dimensional chains of this compound at a Ag(111) surface under UHV conditions; c) proposed arrangement of the molecules within the chains; d) side view showing the tilting of the phenyl rings which allows the intermolecular hydrogen bonds to be formed. Reprinted from Ref. [17].

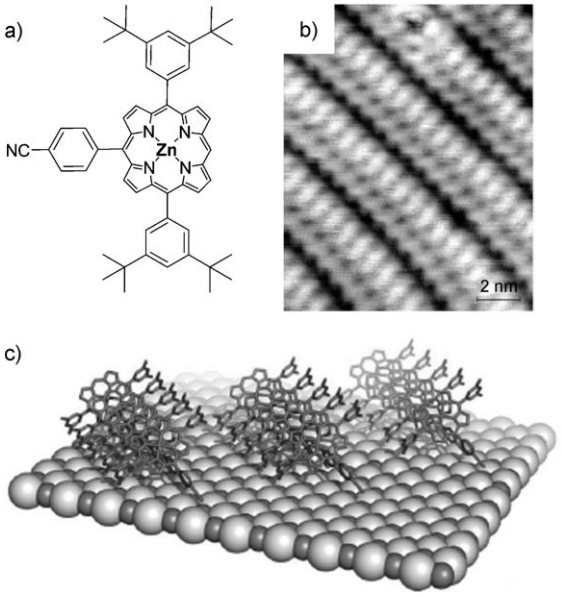

Figure 6. a) Molecular structure of the cyanophenyl-functionalized zinc porphyrin; b) nc-AFM image of a monolayer of parallel porphyrin wires on a KBr(001) surface; c) proposed arrangement of the porphyrin molecules on the surface. Reprinted from Ref. [21].

There are various media from which molecules can adsorb onto the substrate, and these can all have an effect on the resulting molecular organization. The medium, furthermore, strongly determines the deposition conditions and the related thermodynamic or kinetic parameters of the self-assembly process. Many STM studies are performed under inert UHV conditions, where molecules are generally evaporated, or alternatively a solution of them is sprayed onto the substrate by using a spray valve. A key advantage of working under UHV conditions is that one can obtain a superior control over the surface coverage: while at other types of interfaces monolayers are typically formed which tend to fully cover the available surface, under UHV conditions sub-monolayer structures or isolated clusters of molecules can also be studied. In general these structures are kinetically stable as a result of slow interface dynamics, which can even be completely frozen out by lowering the temperature (sometimes even to 4 K). On the other hand, dynamics can be induced by increasing the temperature, and adsorbed molecules can in this way be stimulated to reach a thermodynamically favorable situation by maintaining the temperature for a prolonged period of time at a higher level (annealing). The greatest advantage of UHV–solid interfaces is that they can be obtained in a very clean form, thus allowing the study of compounds that are extremely sensitive to air and moisture.

The interfacial ordering of compounds that are in the liquid or liquid-crystalline state at the temperature at which adsorption occurs can sometimes be probed by simply applying a drop of the material onto the surface. However, the majority of compounds are not liquid or liquid-crystalline. Dissolving them in an appropriate liquid which is then brought in contact with the substrate, sometimes followed by solvent evaporation prior to STM imaging, has become a popular and simple approach to assemble molecules in two dimensions.[22] At a liquid–solid interface, in addition to molecule–molecule and molecule–substrate interactions, the solvent is a factor that cannot be neglected. It is, therefore, remarkable that, despite the fact that numerous STM studies have been carried out on that interface, insight into the role of the solvent in two-dimensional self-assembly processes is so still lacking. The physisorption process of molecules from the liquid to the surface is generally a matter of reaching thermodynamic equilibrium. Dynamics play an important role in the early stages of monolayer formation: molecules continuously adsorb and desorb at the interface, and under ideal conditions the system converges to a minimum overall energy. This can be both a curse and a virtue. A huge benefit is that the possibility of self-repair can lead to perfectly organized arrays of molecules over large distances in the monolayer, but on the other hand, it can take considerable time before such a minimum-energy situation is reached. It should, however, be realized that self-repair and high stability are often at two opposite ends of the scale of intermolecular bonding strength, which means that for two-dimensional self-assembled systems at a liquid–solid interface, a final equilibrium situation might still be dynamic in the sense that molecules at the surface can exchange with molecules in solution. This behavior can be undesirable when the monolayer is meant to perform in a certain function, for example, as a matrix for guest molecules or as a heterogeneous catalyst.

The solvents used in STM studies at liquid–solid interfaces are in most cases chosen for reasons of practical use: they should dissolve the molecules of investigation but not compete with them for adsorption at the surface, they should be chemically inert, and have a low vapor pressure. The low vapor pressure should ensure a stable environment for the two-dimensional self-assembly process, which must not suffer from the continuously changing conditions caused by evaporation. Often, high-boiling organic solvents are used; these have a low polarity so that the tunneling current is not disturbed. This does not, however, mean that STM measurements in highly polar liquids, for example, aqueous solutions, are not possible. By making use of a special type of microscope—an electrochemical STM (EC-STM)—in which two additional electrodes are employed to gain independent control over the electrochemical potentials of the tip and sample, surfaces can be imaged in aqueous conditions with control over the potential.

The molecular systems discussed so far all self-assemble at the UHV–solid or the liquid–solid interface. Processability problems can, however, arise when molecules become so large that thermal cracking occurs during vacuum sublimation, or they become insoluble in conventional liquid media. In such cases, alternative deposition procedures are required, and recently an elegant method to self-assemble large nanographene molecules on a surface was reported, which relies on the soft-landing of ions by solvent-free matrix-assisted laser desorption/ionization (MALDI).[23] By using this method, the nanographenes were first ionized and transferred into the vacuum state by solvent-free MALDI, then purified in a mass spectrometer, and finally deposited on a graphite surface in a specially configured soft-landing unit. After

processing, STM and AFM revealed the presence of highly ordered arrays of nanographenes, oriented in an edge-on geometry with respect to the graphite surface.

It remains a major challenge though to induce self-assembly of insoluble species on a substrate without using modern methods. An exciting new approach for the preparation of surface-supported supramolecular arrays under ambient conditions is by so-called "solid–solid wetting".[24] The technique relies on bringing nanocrystals of a compound in direct contact with a substrate, whereupon layers of molecules disintegrate from the crystalline state and adsorb on to the surface because of a gain in binding energy. The success of this concept was demonstrated by the adsorption of quinacridone, a dye which is a textbook example of a molecule that carries all the information to self-assemble into one-dimensional stacks through hydrogen bonding (Figure 7a). In combination with thermally activated diffusion, the compound self-assembled into highly ordered supramolecular chains at a graphite surface, of which the growth is controlled in a one-dimensional manner (Figure 7b). After deposition, the direction of the supramolecular chains could be easily manipulated by mechanical contact with the STM tip.

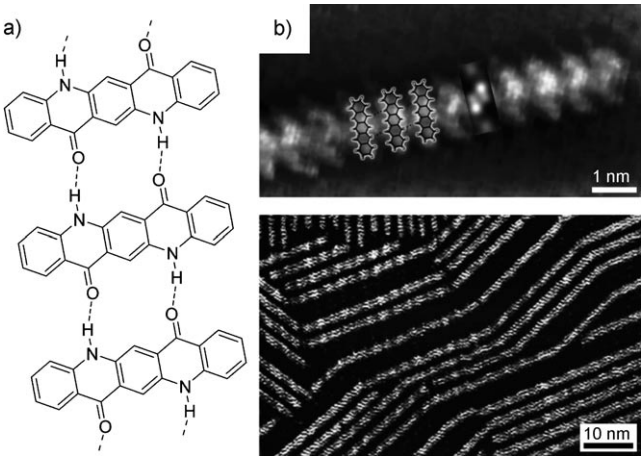

Figure 7. a) Arrangement of quinacridone molecules in a one-dimensional self-assembled chain; b) STM images of quinacridone chains on a graphite surface after application of the solid–solid wetting procedure. Reprinted from Ref. [24].

3. Chirality on Surfaces: Pasteur Would Love It ...

In addition to the traditional tools of supramolecular self-assembly that are used to direct the ordering of molecules on surfaces (see Section 2), the presence or absence of chiral centers in the molecules can have a pronounced influence on the outcome of the self-assembly process. A significant number of publications on supramolecular self-assembly at surfaces deal with chirality. Pasteur realized in 1848[25] that two enantiomers, that is, mirror-image molecules, do not always cocrystallize, but may crystallize in different, although mirror-image-related crystals; an important step was taken in the mechanical (manual) separation of mirror-image molecules. The separation of enantiomers by crystallization is still today the most popular technique used in the pharmaceutical industry. However, roughly only 10% of the racemates can be treated successfully in this way. Studies on two-dimensional crystallization with submolecular resolution can bring insight into the complexity of chiral expression and chiral recognition on surfaces. In addition, chiral surfaces play an important role in enantioselective catalysis and have stimulated research on supramolecular surface chirality.

3.1. Dimers, Clusters, and Monolayers: Chiral Recognition

Getting insight into the processes that are involved in the chiral recognition of molecules that lead to interactions between homochiral or heterochiral pairs of molecules, and the different hierarchical modes of self-assembly leading to homochiral (conglomerate formation) or heterochiral crystals (racemate formation) are important for unraveling the details of supramolecular surface chirality.[26] The first studies dealing with chirality at surfaces were performed more than 10 years ago, and focused on the formation of patterns by pure enantiomers and racemic mixtures at the liquid–solid interface, or at the interface of a liquid-crystalline material and a solid support.[27] Those studies already clearly showed that the chirality of monolayers on surfaces is expressed in two ways, namely, by the ordering of the molecules (5 out of the 17 space groups on the plane are chiral[28]), and by the relative orientation of the molecules with respect to the substrate. A few years later, the first reports appeared which brought unrivaled insight into the details of the chiral expression of molecules—ranging from dimers[29] and clusters[30] to monolayers.[31]

For an object to be chiral, it must not have any inverse symmetry elements, such as reflection planes or a center of symmetry. A special case of chirality can, however, evolve when an interface is involved. In this case, objects become confined to two dimensions, and as a result chirality is more easily achieved, since an interface does not have a center of symmetry and reflection planes can only be maintained normal to it. This implies that objects which are prochiral in three dimensions can become chiral in two dimensions upon confinement on the interface. Enantiomers form mirror-image (also called enantiomorphous) structures on a surface, as long as the presence of the chiral center influences the adsorption of the molecules effectively,[32] because the interaction with the surface leads to the formation of diastereomeric adsorbed states. For example, cysteine enantiomers adsorb as homochiral pairs of D- and L-cysteine, which are mirror images of each other with respect to the symmetry of the underlying gold surface (Figure 8).[29] The chiral recognition in this particular system was explained by a three-point contact model (sulfur–gold, amino–gold, and carboxylic acid–carboxylic acid), but chiral recognition has recently been shown, in general, to be more complex.

Chiral recognition indeed involves more than just the static "lock-and-key" picture.[33] Dynamic mutual conformational adjustments are important when discriminating stereo-

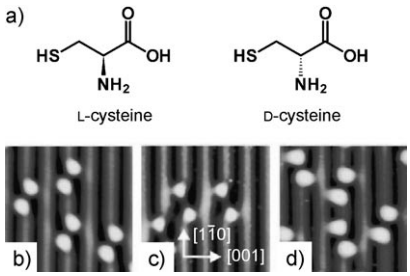

Figure 8. a) Molecular structures of L- and D-cysteine; b) STM image (4.9×5.3 nm^2) of L-cysteine pairs on a Au(110) surface; c) as (b), but of D-cysteine pairs, d) as (b), but from DL-cysteine. Reprinted from Ref. [29] with permission from the Nature Publishing Group.

isomeric molecules. STM studies of individual di(phenylalanine) molecules, which have two chiral centers, on a Cu(111) surface under UHV conditions show that both single molecules and linear supramolecular chains are present at low substrate coverage (Figure 9). A molecule is characterized by

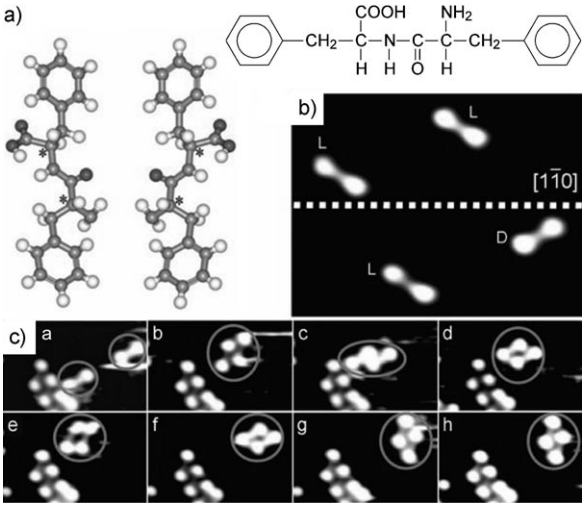

Figure 9. a) left: Molecular models of L-Phe-L-Phe and D-Phe-D-Phe; the asterisks show the stereocenters; right: molecular structure of di(phenylalanine); b) STM image (8.3×6.4 nm^2) of individual di(phenylalanine) molecules showing that the two enantiomers are mutual mirror reflections with respect to the plane perpendicular to the surface through the [1−10] axis; c) series of STM images (a–h) showing the formation path of a homochiral pair of molecules (in circles). Reprinted from Ref. [33].

two bright protrusions (the phenyl groups) and a dimmer central part. The main axis through the bright protrusions is rotated with respect to the long supramolecular chain axis. Experiments on the enantiopure compounds show that the supramolecular chains are homochiral and that the different enantiomers are rotated by an angle with the same absolute value, but with opposite sign. Moreover, the orientation of single adsorbed molecules is not random: Isolated enantiomers appear as mirror images with respect to a plane through the [1$\bar{1}$0] axis. These observations show that the stereogenic centers are involved in the interaction between the molecule and the substrate. The absolute configuration of isolated molecules and of those that are part of supramolecular chains can be deduced from their orientation with respect to the substrate.

Theoretical models revealed that the difference in the orientation of isolated molecules and molecules in supramolecular chains on the substrate are related to different molecular conformations in both states, and that isolated molecules undergo a conformational change when they become part of the supramolecular chain. The stereoselective self-assembly of adsorbed di(phenylalanine) enantiomers into molecule pairs and chains occurs through mutually induced conformational changes. This behavior was confirmed in a unique STM experiment in which the interaction and dynamics of individual molecules during formation of the dimers was observed (Figure 9c). After the molecules had met, a first change in their adsorption geometry was observed and a metastable pair was formed. Only after several further rearrangements was a stable situation reached in which the arrangement of the molecules within the pairs was identical to that observed in the homochiral pairs. Stable heterochiral pairs were not formed. The difference between interactions between homochiral and heterochiral pairs and the dynamics involved are sufficient to bias the formation of homochiral tapes.

Not only chiral, but also achiral molecules can self-assemble into chiral domains. Certain achiral molecules are described as prochiral—one desymmetrizing step away from chirality—if they become asymmetric when they are constrained on a surface.[34] Other molecules remain achiral upon deposition at a surface, but nevertheless form chiral two-dimensional structures.[35] This is not a consequence of (just) molecular asymmetry, but the result of intermolecular and molecule–substrate interactions. Similar to chiral molecules, prochiral molecules have a strong tendency to form conglomerates. The packing of one (two-dimensional) stereoisomer with copies of itself is thermodynamically more favorable (or kinetically faster) than packing with other molecules.[36] Here, one should note that the emergence of supramolecular chirality relies on the efficient transfer of chiral information (which in the case of prochiral molecules, only arises when constrained on a surface) from one molecule to the next by the formation of a sufficiently large number of intermolecular contact points within one domain. Only under this prerequisite is a domain with a well-defined chiral signature formed. This is demonstrated in an impressive way by the self-assembly of stilbene dicarboxylic acid on Cu(100).[37] This prochiral molecule self-assembles into enantiomerically pure hydrogen-bonded homochiral phases. The metal-coordinated counterparts, however, give rise to networks with randomly arranged enantiomeric building blocks, which might be attributed to the large spacing of the now isolated molecules.

Most STM studies have provided a static picture of the outcome of the self-assembly process, with lateral mass transport of these prochiral molecules invoked to explain the segregation of both enantiomeric forms into separate domains. However, this is not the only possible mechanism.[38] Conformational dynamics were shown to be at play in the self-assembly of organic prochiral molecules that switch

between enantiomeric forms as they undergo thermally induced conformational changes. Figure 10 shows the self-assembly behavior of a molecule which upon rotation around an acetylene bond can form LR/RL, LL, and RR conformers

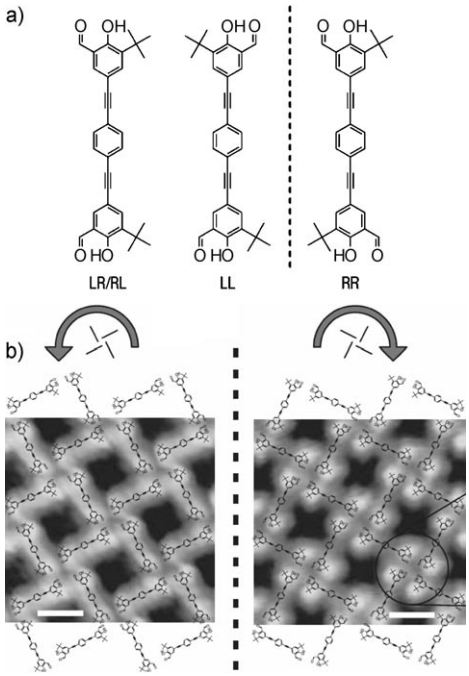

Figure 10. a) Molecular structure of three different conformers (LL, RR, and LR/RL); LL and RR are enantiomers; b) STM images (scale bar: 2 nm) of network structures of opposite chirality, as seen from the sense of rotation of the windmill motif. Reprinted from Ref. [38] with permission from the Nature Publishing Group.

on a Au(111) surface under UHV conditions. The dominating motif in one of the phases is a windmill-like arrangement of four molecules adsorbed with their backbones parallel to the substrate. The windmill pattern is chiral, with the bright *tert*-butyl groups completely ordered in the network phase. They are always positioned at the side of the molecular backbone, pointing away from the central node, and as a result, there is a direct correlation between the chirality of the tiling and the orientation of the surface conformers. Mirror-image domains are formed, which consist exclusively of LL or RR conformers. Time-separated STM images show that incoming RL conformers change their conformation at the domain edges to fit the domain chirality.

3.2. Enantiopure Monolayers

At high surface coverage, STM images of (*R*,*R*)-tartrate molecules on a Cu(110) surface under UHV conditions revealed their self-assembly in enantiomorphous rows of three, with each row stacking parallel to other rows to form long chains (Figure 11).[31] The growing direction of the rows does not coincide with one of the symmetry axes of the underlying metal surface, which implies the creation of a

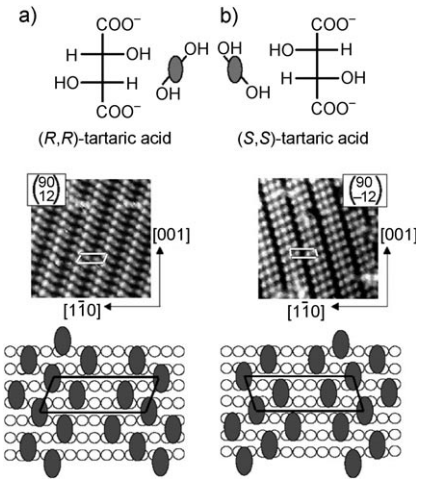

Figure 11. Molecular structure, STM images (10.8×10.8 nm^2), and schematic arrangements of a) (*R*,*R*)-tartaric acid monolayers and b) (*S*,*S*)-tartaric acid monolayers on Cu(110). Reprinted from Ref. [31] with permission from the Nature Publishing Group.

chiral surface that is nonsuperimposable on its mirror image. DFT calculations suggest that this self-assembly is governed by through-space and/or through-metal lateral interactions. (*R*,*R*)- and (*S*,*S*)-tartaric acid form identical two-dimensional patterns, which are, however, related by mirror symmetry. In this case, which involves chemisorption, there is a direct transfer of chirality at the molecular scale to chirality at the macroscopic scale, and involves different hierarchical levels:

1) preservation of the chiral centers upon adsorption,
2) adsorption-induced chiral distortion of the molecular backbone,
3) organization of adsorbates into a chiral arrangement that breaks the mirror symmetry of the underlying Cu(110) surface,
4) adsorption stress which leads to the creation of vacant chiral channels between the adsorbed molecules.

In addition to interactions between enantiomers, interactions between dissimilar species are also important.[39]

We have already touched on the importance of chiral molecular recognition in the formation of homochiral assemblies. When a racemic mixture condenses, it can do so in three different ways:

1) as a racemate, where both enantiomers are part of the same crystalline domains,
2) as a conglomerate, where both enantiomers appear in mirror-image domains,
3) as a "solid solution", in which disordered domains contain both enantiomers.

For most compounds, a mixture of enantiomers will segregate into enantiopure domains, or prochiral molecules will separate into domains where all the molecules have the same enantiotopic face directed to the substrate. There are some interesting examples, however, where chiral separation into different domains does not take place.[40]

3.3. Prochiral Molecules

Zimmt and co-workers described an elegant system in which the stereochemical morphology of monolayers of prochiral molecules switches from a two-dimensional racemate to a two-dimensional conglomerate; this was achieved simply by elongating the alkyl chains with one methylene unit.[41] Two 1,5-bis-(3′-thiaalkyl)anthracene derivatives (Figure 12a) with linear alkyl chains containing either 11 or 12 carbon atoms were adsorbed at the interface of graphite and 1-phenyloctane. The STM images of the monolayers formed by the two compounds revealed a striking difference in the organization. The anthracene moieties in the compound with the C_{11}-alkyl chains alternate from row to row, thereby leading to a racemic monolayer with *pg* plane-group symmetry (Figure 12c). In contrast, the orientation of the anthracene moieties in the compound with the C_{12}-alkyl chains is constant within a given domain, which reflects the formation of a two-dimensional conglomerate monolayer with *p*2 plane-group symmetry (Figure 12b). Isolated mirror-image two-dimensional enantiomers have identical energy, while pairs of interacting two-dimensional isomers are diastereomeric and, therefore, have distinct energies. The two-dimentional chirality of the anthracene moieties within the same row is identical, and apparently of the lowest energy, for both compounds. The difference between the two compounds is expressed in terms of the difference in their relative orientation in adjacent rows.

But what determines this difference? The organization of the molecules within the monolayer is governed by both molecule–molecule and molecule–substrate interactions. Alkyl chains tend to align along one of the main symmetry axes of graphite and methylene groups of adjacent chains align in registry to maximize the intermolecular van der Waals interactions. The different stereomorphologies are proposed to arise from a different relative orientation of the CH_2–CH_3 and the C–aryl–C1′ bonds within the same side chain. both bonds are oriented parallel in the compound with C_{11} chains, while they make an angle of about 110° within the same chain in the compound with C_{12} chains. Optimization of the van der Waals interactions between the chains, in combination with their favorable all-*trans* conformation, then leads to the difference in the orientation of the anthracene moieties in adjacent rows.

A related case was observed under UHV conditions. At low coverage on a Cu(110) surface, achiral succinic acid molecules adsorb into enantiomorphous domains with a structure that is remarkably similar to the tartrate phase discussed above. At high coverage (0.25 monolayers) and upon heating to 473 K, succinic acid (SU) adsorbs into rows along the [001] direction of Cu(110) (Figure 13).[42] Adjacent rows differ in their molecular orientation: the molecules have an oval shape, with the long axis rotated by +65° (D-SU) or −65° (L-SU) with respect to the [001] direction. In principle, the two molecular orientations reflect two distinguishable local chiral motifs, each being the mirror form of the other. Therefore, the unit cell is heterochiral, while the overlayer is racemic but composed of homochiral chains.

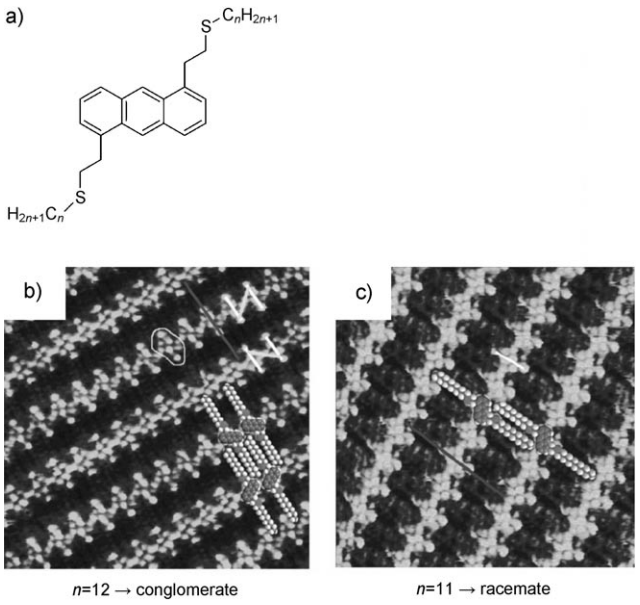

Figure 12. a) Molecular structure of the anthracene derivatives; b) STM image (11×11 nm²) of a monolayer of the compound with C_{12}-alkyl chains at the interface of graphite and 1-phenyloctane; the anthracene moieties are oriented in a parallel fashion in adjacent rows, thereby resulting in a two-dimensional conglomerate; white bars indicate S-S distances within a single molecule; the circled region indicates the core of a molecule; the gray line indicates the length of a molecule; c) STM image (12×12 nm²) of a monolayer of the compound with C_{11}-alkyl chains; the anthracene moieties are oriented in a twisted fashion in adjacent rows, thereby giving a 2D racemate; the white bar indicates the S-S distance within a single molecule and the gray line the length of a molecule. Reprinted from Ref. [41] with permission from the American Chemical Society.

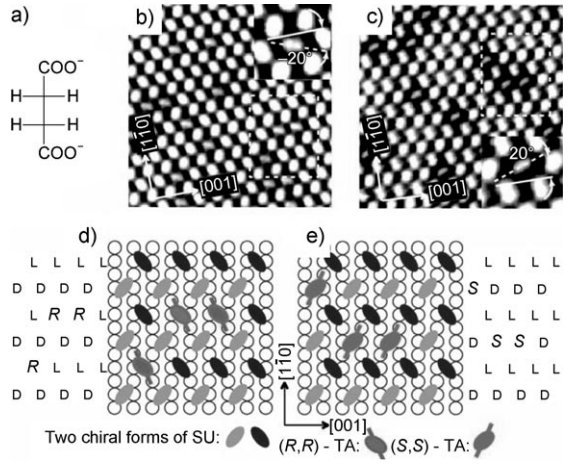

Figure 13. a) Structure of the succinate dianion (SU); b, c) topographic STM images (8.0×8.0 nm²) of (*R*,*R*)- and (*S*,*S*)-tartaric acid (TA) substitution, respectively, in a SU monolayer on Cu(110); dotted white box: area corresponding to the models in (d) and (e), respectively. The angle of the long axis of tartaric acid with respect to the [001] direction is indicated in the enlarged images; d) schematic representation of the adsorption sites occupied by (*R*,*R*)-tartaric acid (*R* in the figure); e) as (d), but with (*S*,*S*)-TA (*S* in the figure). L = L-Su, D = D-SU. Reprinted from Ref. [42].

The organization of a racemic mixture of succinic acid molecules is not changed upon coadsorption of (*R*,*R*)-tartaric acid, and some (*R*,*R*)-tartaric acid molecules become incorporated within the structure in sites corresponding to succinic acid molecules. A surprising result, however, is that (*R*,*R*)-tartaric acid molecules only occupy L-SU but not D-SU sites, while the opposite is the case when (*S*,*S*)-tartaric acid is used (Figure 13 d,e). According to DFT calculations, different intra- and intermolecular hydrogen bonds and molecular-backbone distortions are responsible for the observed site preference of the (*R*,*R*)-tartaric acid molecules. The site-specific chiral recognition within a two-dimensional heterochiral lattice leads to a highly enantiospecific substitution of a dissimilar chiral guest.

3.4. Racemates: Homo- and Heterochirality

When enantiopure heptahelicene molecules are forced into a close-packed monomolecular layer under UHV conditions, molecular chirality is transferred to monolayer chirality (Figure 14).[43] Repulsive forces dominate the lateral interactions when the molecules are squeezed together. The self-assembly is clearly not only governed by the interaction between the molecules, but also by adsorbate–substrate interactions, which determine the mobility of the molecules on the surface. On Cu(111) and at 100 % surface coverage, the unit cell of the adsorbate lattice contains a group of three molecules in a cloverleaf structure. The observed adsorbate lattice structures show enantiomorphism: adsorption of the *P* enantiomer of the helicene leads to structures which are mirror images of those observed for the *M* enantiomer. In addition to the chiral shape of the unit cell, the arrangement of the molecules within the unit cell is also chiral.

Interestingly, mirror domains (labeled λ and ρ) have been observed at the same surface for the racemate. Intuitively, one would assume then that conglomerate formation has taken place, but this is, however, not the case. STM experiments in combination with molecular modeling studies showed that heterochiral *M*-*P* pairs become aligned in a chiral configuration in zigzag rows. It came, however, as a surprise that a small enantiomeric excess leads to the disappearance of one of the two mirror domains.[44] An excess of the *M* helicene favors the formation of λ-domain pairs and an excess of the *P* helicene gives ρ-domain pairs. Only λ domains or ρ domains are observed, depending on the helicity of the excess helicene, from an enantiomeric excess of 0.08 and higher. In this case, lattice homochirality results over the entire surface, that is, only domains of the same handedness, composed of chains of heterochiral pairs, are observed.

As the ratio of the two enantiomers on the surface must remain constant, the enantiomeric excess must be located outside the domains in the disordered areas. At domain boundaries, these excess molecules influence the relative alignment of the heterochiral pairs at domain edges, which is amplified throughout the racemic crystalline domain in a cooperative fashion. Key to this cooperative process is the ease by which a transition of one mirror domain to the other can be realized, since it requires only a change in the relative position of both enantiomers of a heterochiral pair.

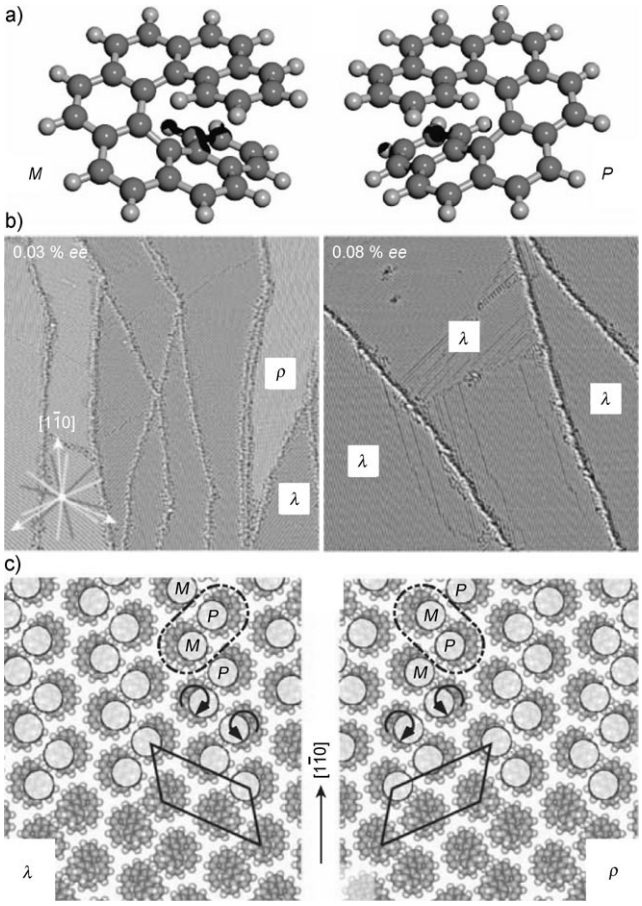

Figure 14. a) Molecular models of the (*M*)- and (*P*)-heptahelicenes; b) representative series of STM images (200×200 nm^2) with an increasing enantiomeric excess of heptahelicene molecules on a Cu(111) surface under UHV conditions. At *ee* = 0.08, the ρ domains have completely disappeared and only λ domains are observed; c) lattice structures (λ domain (left), ρ domain (right)) of the two lowest energy configurations of racemic heptahelicene obtained from molecular mechanics calculations. Pale circles highlight the top-most parts of the molecules which are expected to be brightest in the STM images. The dashed ovals indicate heterochiral *M*-*P* pairs (molecule–molecule distance: 9.2 Å) which form the basic building blocks of the zigzag rows; black boxes: unit cells. Reprinted from Ref. [44] with permission from the Nature Publishing Group.

3.5. Role of the Solvent

As was already briefly mentioned in Section 2.2, the role of the solvent in the self-assembly of molecules into a two-dimensional lattice at a liquid–solid interface is still rather unclear. It can, however, be expected that the solvent will be participating in many two-dimensional self-assembly processes, in particular in cases where supramolecular interactions (for example, hydrogen bonding) can occur between the solvent molecules and the adsorbed molecules. When in such a case the solvent is chiral, this can lead to the emergence of macroscopic chirality within self-assembled monolayers of

achiral molecules at an achiral surface. A recent example of such a solvent-mediated process is the self-assembly of an achiral oligo(*p*-phenylene vinylene) (OPV) derivative functionalized with a triazine moiety (Figure 15a) at the interface of graphite and the enantiomerically pure solvents (*R*)- and (*S*)-1-phenyl-1-octanol (Figure 15b).[45] STM studies revealed that rosette structures were formed (Figure 15c), and from statistical studies of large-scale images it was concluded that there was a clear bias towards counter-clockwise (CCW) rotating rosettes when (*R*)-1-phenyl-1-octanol was used, whereas clockwise (CW) rotating rosettes were favored in the case of (*S*)-1-phenyl-1-octanol. Figure 15d,e shows that both the CW- and the CCW-rotating rosettes are arranged in arrays in which they are oriented differently relative to the rosettes in the adjacent arrays. This is highlighted by the sequence of dashed and solid white lines which connect the terminal phenyl groups of similarly oriented OPV units along the unit cell vector *b*. Their sequence and relative orientation highlights the chiral nature of the entire monolayer. Although the solvent molecules are not coadsorbed, hydrogen-bonding interactions between their hydroxy groups and the hydrogen-bond acceptors of the OPV molecules are believed to be of key importance for the induction of the observed homochirality at the surface (Figure 15f). The actual mechanism of chiral selection that favors the formation of rosettes with a particular handedness during the formation of the monolayer is not known as yet, but in addition to solvent–solute interactions it can also involve desolvation processes that are more facile with one chirality and steric restrictions within the monolayer so that a particular ordering is favored, or, most probably, a combination of all of the above factors.

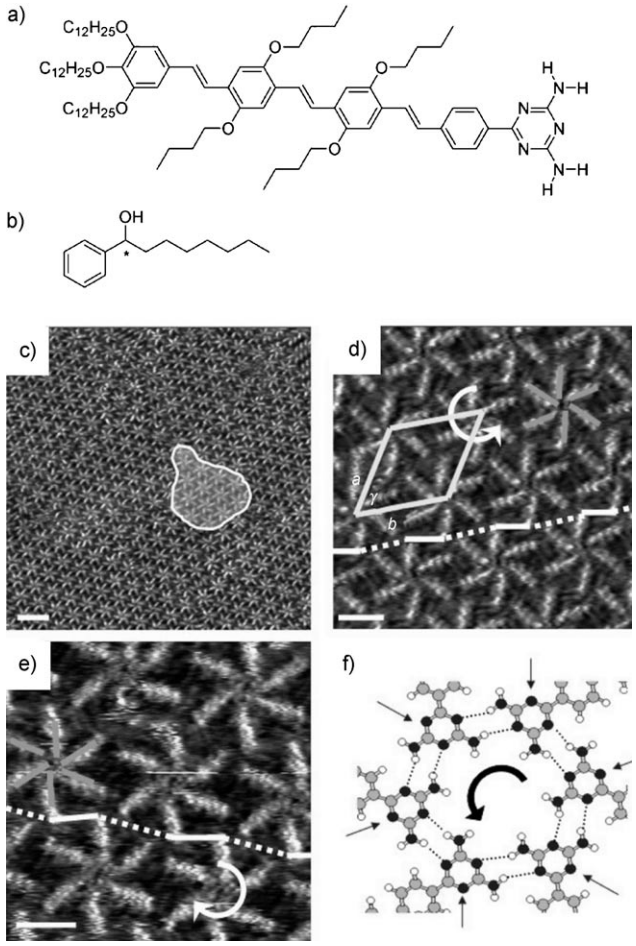

Figure 15. a) Molecular structure of the achiral OPV molecule; b) molecular structure of the chiral solvent 1-phenyl-1-octanol; c) STM image of a monolayer of rosettes formed by OPV molecules at the interface of (*R*)-1-phenyl-1-octanol and graphite; a small domain of CW-rotating rosettes within a large domain of CCW-rotating ones is marked; scale bar: 10 nm; d) as (c), but with magnification, with the unit cell (light gray lines) and orientation of the OPV molecules within a rosette (dark gray lines) indicated; the sequence of dashed and solid white lines indicates the orientation of rosettes relative to those in adjacent rows; scale bar: 3 nm; e) as above, but the same molecule at the interface of (*S*)-1-phenyl-1-octanol and graphite; scale bar: 3 nm; f) proposed hydrogen bonding motif of the OPV molecules within a single rosette; arrows indicate hydrogen-bond acceptors which are available for interactions with the chiral solvent. Reprinted from Ref. [45].

3.6. External Stimuli

A fundamentally new method to influence the chiral organization of molecules at a liquid–solid interface, which also does not involve any form of chiral input, is the use of a magnetic field. The success of this approach has been demonstrated by a study of 4-cyano-4′-octylbiphenyl on graphite.[46] This compound is achiral, but the rotation about the C_{alkyl}–C_{aryl} bond is quenched upon its adsorption on a surface, which results in a breaking of the symmetry and the generation of enantiomorphic domains in two dimensions. The mirror-related right-and left-handed molecular domains which are thus formed at the liquid–solid interface can be easily recognized in STM images.

A thin film of this compound, which is a smectic liquid crystal at room temperature, was heated and subsequently cooled on a graphite surface in the presence of a magnetic field of 1.2 T which was oriented parallel to the substrate plane. As a result of this field, the orientational order induced in the bulk material was imprinted on the monolayer at the surface, thereby resulting in a molecular film with macroscopic uniform in-plane alignment. When the magnetic field direction was rotated, one packing became more favored than the other, and as a result the overall racemic nature of the surface was broken by producing a monolayer with a net excess of one enantiomorph over the other.

4. Nanoporous Supramolecular Networks

4.1. Formation of Nanoporous Networks

A special class of well-ordered two-dimensional networks—namely, those containing void spaces—is gaining increasing attention in recent years.[7,47] These so-called 2D nanoporous supramolecular networks are of interest because they either expose active surface sites selectively at the nanometer level, or they allow decoration of a surface with functional moieties in a spatially defined order. In general,

these porous networks are sustained by rather weak and reversible supramolecular interactions, so that the system is under thermodynamic control and exhibits a substantial degree of dynamic behavior and self-repair. In the ideal case, highly ordered and defect free assemblies may be obtained.

4.1.1. *Nanoporous Networks by Hydrogen Bonding*

Many of the nanoporous supramolecular networks described so far are based on self-assembly through intermolecular hydrogen bonds, as has already been mentioned briefly in Section 2.1 for the networks formed by trimesic acid (TMA) both under UHV conditions[6,48] and at liquid–solid interfaces.[49] Two polymorphs, which are referred to as the "chicken wire" or "honeycomb" structure (Figure 16a) and the "flower" structure, are mainly found at the liquid–solid interface. Which of the polymorphs is formed depends on the nature of the solvent, but in both cases the pore walls are composed of six TMA molecules that are connected through double hydrogen bonds between the carboxylic acid moieties. While only hydrogen-bonded dimers of TMA are present in the honeycomb network, a trimeric hydrogen-bonding mode occurs in the flower structure, which leads to a closer molecular packing. Under UHV conditions, other polymorphs with even higher density were found, the most dense being a hexagonal pattern containing exclusively hydrogen-bonded trimers. Although the distances between the pores in the two main polymorphs are different, their size is the same (ca. 1.2 nm in diameter).

With the aim of increasing the pore size, trifunctional benzene molecules were investigated in which the carboxylic acid functionalities were connected to the central core through spacers. 4,4′,4″-Benzene-1,3,5-triyltribenzoic acid (BTB), for example, forms a honeycomb network with pores with an internal diameter of 2.9 nm both on a Ag(111) surface under UHV conditions[50] and at the liquid–graphite interface (Figure 16b).[51] TMA and its rigid extended derivatives give rise to highly stable and symmetric networks, but sometimes network structures are also desired which have pores with a different or adaptable symmetry. Such networks have been obtained by making use of 1,3,5-tris(10-carboxydecyloxy)benzene (TCDB) as the building block, with flexible spacers between the core and the carboxylic acid functions. It forms porous networks on a graphite surface, in which two of the carboxylic acid groups of each molecule are hydrogen bonded to a neighbor to form a pseudo-rectangular pore, whereas the third carboxylic acid dimerizes with the carboxylic acid of a more distant TCDB molecule through formation of hydrogen bonds.[52]

In an alternative approach, isophthalic acid derivatives were connected through rigid spacers to give tectons that can be regarded as analogues of a hydrogen-bonded TMA dimer.[53] At the heptanoic acid–graphite interface, a "short" tecton in which the isophthalic acid moieties are connected by a single C–C bond forms parallel networks of cyclic tetramers exclusively, while a tecton with an extended spacer self-assembles into a Kagomé network (Figure 16c). The difference in the self-assembly behavior could not be explained by differences in the packing density or the number of hydrogen bonds formed, which are identical for both polymorphs. DFT/B3LYP calculations, however, predicted that the hydrogen

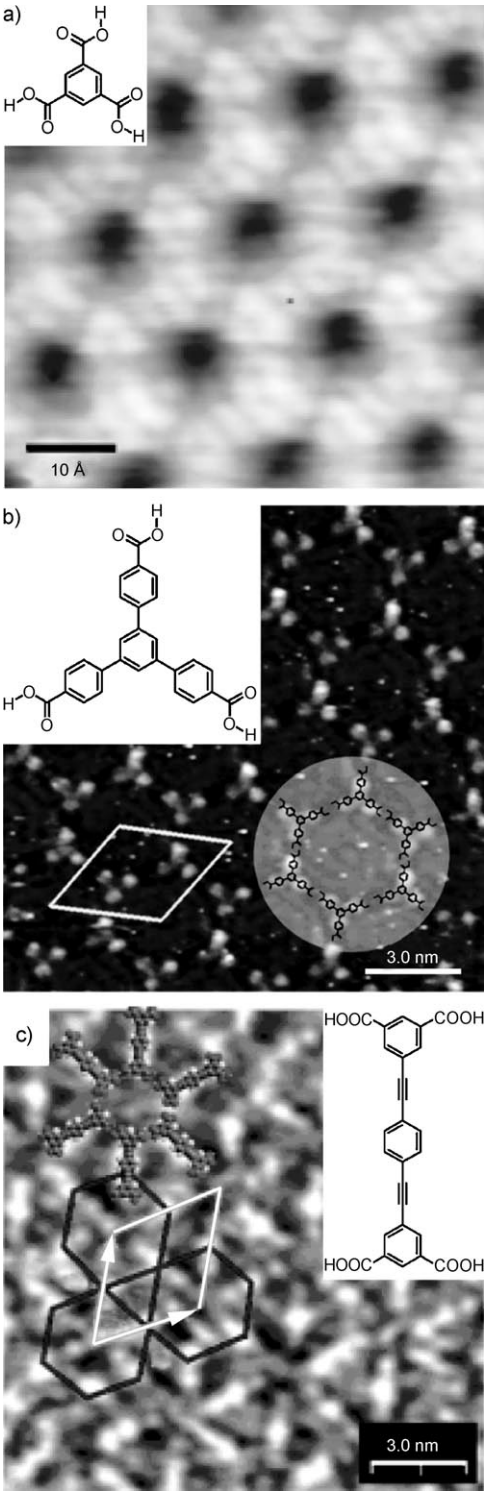

Figure 16. STM images of two-dimensional supramolecular nanoporous networks formed by a) TMA (honeycomb polymorph), b) BTB (white box: unit cell), and c) a tecton with two isophthalic acid units; white box: unit cell; dark lines: kagomé lattice. Reprinted from Ref. [6] as well as from Refs. [51] and [53] with permission from the American Chemical Society.

bonds for the "short" tecton in a parallel network are stronger than when the molecules would be arranged in a Kagomé network. The elongated tecton, in contrast, was estimated to be more stable in the Kagomé network.

Another striking example is the assembly of linear dicarbonitrile-polyphenyl species NC-Ph_n-CN ($n = 3$–5), on a Ag(111) surface (Figure 17).[54] These simple, linear ditopic molecular building blocks form regular networks with increasing complexity upon increasing the number of phenyl spacers: NC-Ph_3-CN forms a densely packed "chevron" pattern, while the addition of one phenyl group to the backbone (NC-Ph_4-CN) leads to an open rhombic network. The further addition of an extra phenyl group (NC-Ph_5-CN) results in even more complex packing, namely, a two-dimensional chiral Kagomé lattice. This fascinating change of supramolecular surface patterns with the length of the building blocks arises from the interplay between substrate epitaxial fit, noncovalent lateral interactions, and the conformational flexibility of the molecules.

It is sometimes much more difficult to predict whether a certain molecule will self-assemble into a nanoporous network on a surface. This is illustrated by the adsorption of anthraquinone (AQ) molecules on a Cu(111) surface under UHV conditions, where they arrange themselves into a honeycomb network with pores of about 5 nm in diameter (Figure 18a).[55] Each pore wall is composed of 18 AQ molecules, which enclose more than 200 uncovered Cu atoms. Detailed analysis of the STM images in combination with molecular modeling studies indicated that the vertices of the pores are stabilized by attractive C–H···O hydrogen-bonding interactions between the carbonyl groups and protons coupled to the arene rings of a trimer of neighboring AQ molecules (Figure 18b). It remained, however, unclear why each of the sides consists of exactly three AQ molecules. A key observation was that only parallel lines of AQ molecules were present at low surface coverage, which never came in proximity (< 5 nm) to one another. This finding suggests long-range repulsive interactions, which at low surface coverage prevent the assembly of AQ into trimers and favor the formation of rows, while at high surface coverage they also prevent a closer packing of the arrays in favor of a more-even distribution of the adsorbates in a honeycomb pattern.

Commensurate building blocks can be connected through multiple hydrogen bonds to further increase the robustness of nanoporous networks. In an illustrative example, melamine was coadsorbed with tetracarboxylic diimide (PTCDI) on a silver-terminated silicon surface (Ag/Si(111)) to afford an open honeycomb network (Figure 18c,d).[56] The trifunctional melamine molecules form the vertices of the network, while the straight edges are occupied by PTCDI molecules. The compatibility of the geometries of the two molecules results in three hydrogen bonds per melamine–PTCDI heterodimer, as compared to only two for PTCDI or melamine homodimers.

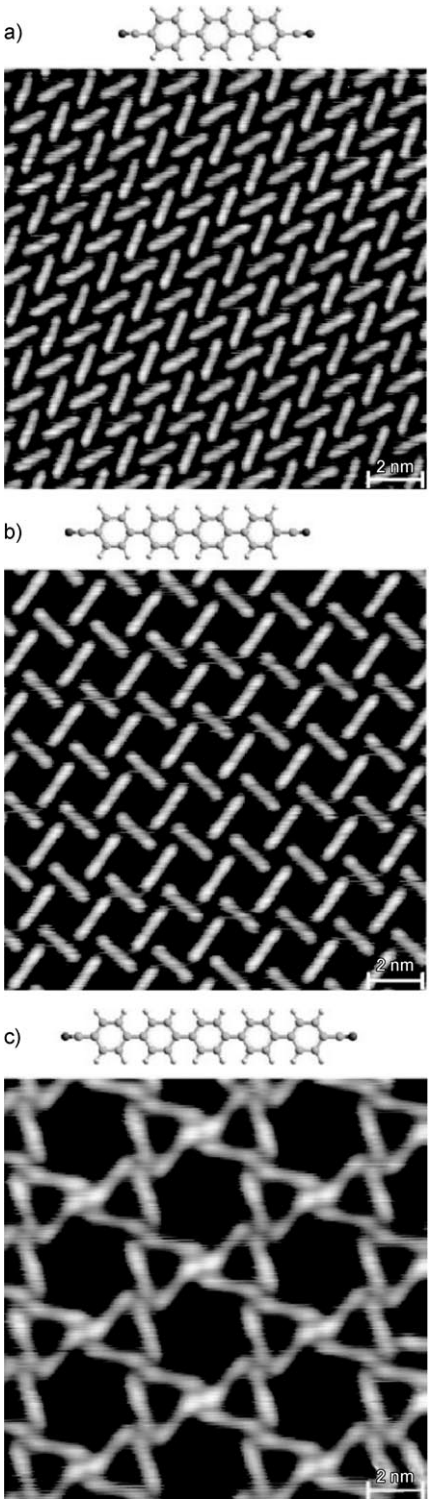

Figure 17. Supramolecular surface patterns with increasing complexity through extension of molecular building blocks on the Ag(111) surface; a) densely packed "chevron" pattern of NC-$(C_6H_4)_3$-CN; b) open rhombic network of NC-$(C_6H_4)_4$-CN; c) chiral Kagomé network of NC-$(C_6H_4)_5$-CN. The respective lengths of the molecular building blocks are 1.66, 2.09, and 2.53 nm. Reprinted from Ref. [54] with permission from the American Chemical Society.

4.1.2. ***Nanoporous Networks by Metal–Ligand Coordination***

Besides through hydrogen-bonding interactions, nanoporous networks can also be constructed by metal–ligand coordination. Since metal–ligand interactions are generally stronger than hydrogen bonds, it is important that they exhibit

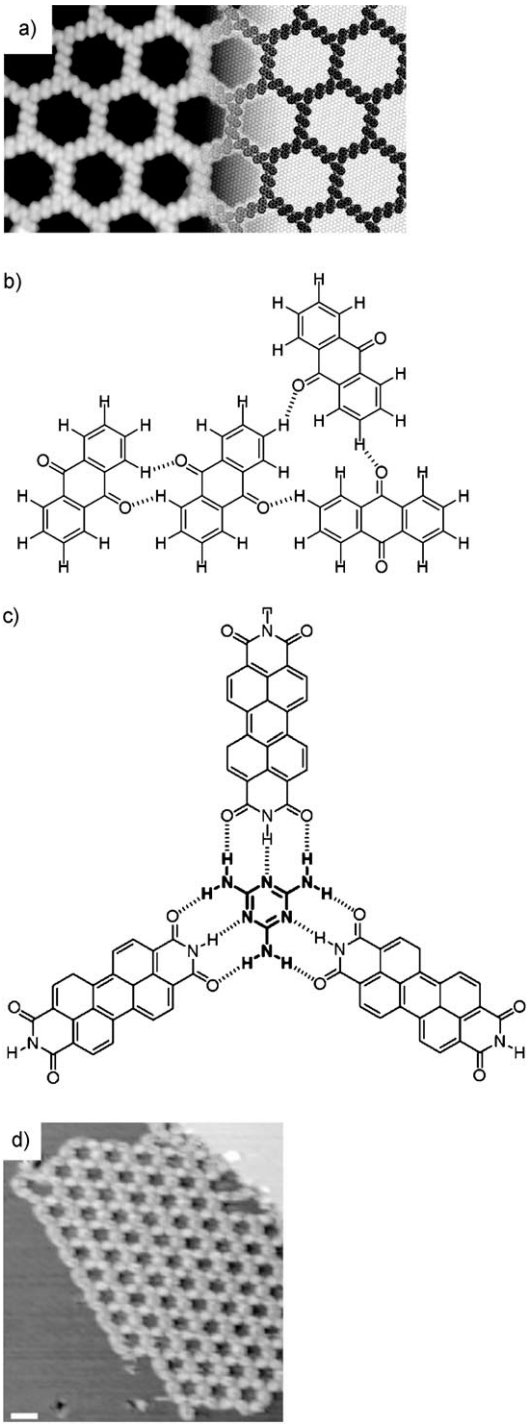

Figure 18. a) STM image (26×15 nm^2) of the honeycomb network formed by AQ on a Cu(111) surface under UHV conditions; a modeled representation of the surface and the adsorbed molecules is drawn in the right part of the image; b) arrangement of the self-assembled AQ molecules forming a row (left) and a vertex (right); c) arrangement of melamine (bold) and PTCDI in a hydrogen-bonded junction of a honeycomb network; d) STM image of this network on a Ag/Si(111) surface under UHV conditions; acale bar: 3 nm. Reprinted from Refs. [55] and [56] with permission from American Association for the Advancement of Science and the Nature Publishing Group.

sufficient reversibility under the self-assembly conditions, which is an essential condition when ordered networks over a long range are to be obtained.

Carboxylic acids have proven to be very useful tectons in metal–organic frameworks (MOFs). Upon adsorption at a Cu(100) surface under UHV conditions, terephthalic acid (TPA), trimellitic acid (TMLA) or 4,1′,4′,1″-terphenyl-1,4″-dicarboxylic acid (TDA) undergo deprotonation upon coordination to added Fe atoms.[57] STM studies revealed the formation of MOFs with different morphologies depending on the stoichiometry of the components, and in all cases their symmetry and shape was induced by the atomic arrangement of the underlying atomic lattice of the substrate (Figure 19).

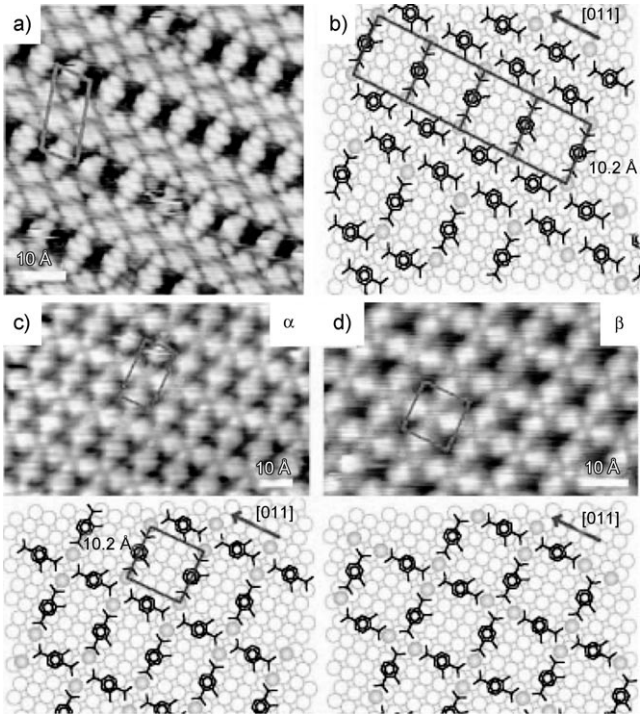

Figure 19. a) STM image of a "double-row MOF" on a Cu(100) surface formed by TMLA and Fe atoms at a coverage ratio of one Fe atom per ligand; rectangle: ladder structure; b) corresponding model; c,d) STM images showing two different phases (α and β) of "single-row MOFs", built from the same components but with the coverage ratio increased to two Fe atoms per ligand; rectangles: ladder structure. The corresponding models of these phases are shown below the images. Reprinted from Ref. [57].

Although a distorted fourfold coordination was observed for each Fe atom, the ligand/metal ratios appeared to be different in the networks. Despite the presence of extra side groups, the MOF formed by TMLA and Fe was found to be almost identical to the MOF formed from TPA and Fe, thus implying that the *ortho*-carboxylate group of the ligand does not participate in formation of the network. However, these still available groups provide the network with highly reactive functional groups to further modify the network cavities.

In general, the structures of two-dimensional MOFs are predetermined by the properties of the ligand and the

electronic characteristics of the metal ions. However, in the confined space on a surface, the realization of a given coordination algorithm might be changed by the presence of a metal substrate, which results in different coordination geometries for the same metal–ligand couple compared to the three-dimensional situation.[58] Unusual threefold symmetric networks are formed when iron centers are coordinated to linear 4,4′-biphenol ligands, or cobalt centers to 1,4′,4′,1″-terphenyl-4,4″-dicarbonitrile ligands under UHV conditions, despite the fact that these metal centers normally exhibit a fourfold coordination symmetry in the bulk phase (Figure 20).

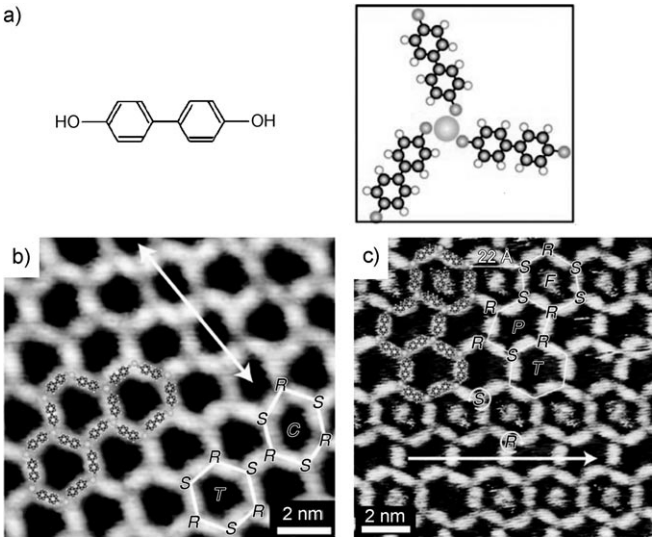

Figure 20. a) Molecular structure of biphenol and a model of the threefold binding of a {Fe(biphenolate)$_3$} motif (which is intrinsically chiral); b,c) STM images of the hexagonal iron–biphenolate networks assembled on Ag(111) and Cu(100) surfaces, respectively, with tentative models superimposed. *R* and *S* denote the clockwise and anticlockwise folding, respectively; arrows: rows of high symmetry. Reprinted from Ref. [58].

By using substrates with different symmetry, namely, Ag(111) and Cu(100), it was proven that the observed threefold coordination symmetry is intrinsic to metal–ligand coordination and not a result of geometrical templating effects of the underlying surfaces. The unusual coordination geometries and stoichiometries are attributed to a rehybridization of the orbitals (and as a result maybe unusual redox states) of the metal centers by the underlying substrates.

A recent report shows that Cu can also exhibit threefold coordination on the surface when coordinated with pyridyl ligands, and this coordination motif is sufficiently strong to compete with substrate interactions.[59] The coordination of Cu adatoms to 5,5′-bis(4-pyridyl)(2,2′-bipyrimidine) on the different substrates Cu(100), Ag(100), and Ag(111) produces similar open networks. A slight distortion of the coordination configuration can compensate for the differences in the commensurability with the substrate, thus highlighting both the robustness and flexibility of this threefold coordination.

4.1.3. Nanoporous Networks by Van der Waals Interactions

The highly specific and directional nature of hydrogen bonds and metal–ligand coordination bonds makes them popular tools to guide the self-assembly of building blocks both in the bulk phase and at an interface. Van der Waals interactions, although occurring ubiquitously between molecules, are far less specific, but at a surface the confinement to two dimensions might endow directionality, especially when the building blocks are rigid. An example of such behavior is the surface assembly of a trimeric "molecular motor" whose structure is shown in Figure 21 a. After deposition from a saturated solution in 1-phenyloctane, the enantiomerically pure compound forms a honeycomb network on HOPG

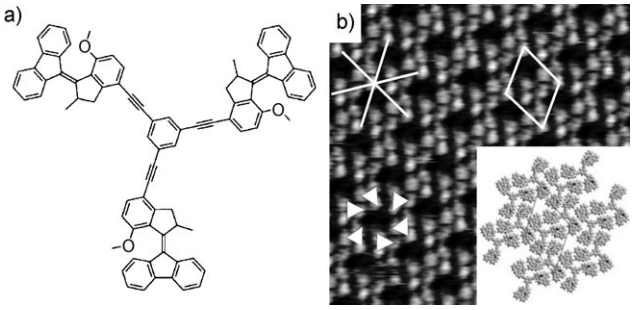

Figure 21. a) Molecular structure of a trimeric molecular motor; b) STM image (18.2×18.2 nm^2) of a honeycomb network formed by the trimeric motor at a 1-phenyloctane–graphite interface; each overlaid triangle represents one molecule (bottom left). The unit cell of the honeycomb (top right) and main crystallographic directions of the substrate (top left) are indicated. A molecular model is shown in the inset. Reprinted from Ref. [60].

(Figure 21 b). The asymmetry of the trimer is expressed both at the molecular level through the orientation of the molecule with respect to the substrate and at the supramolecular level by the clockwise packing of the honeycomb pattern. Only weak van der Waals interactions exist between these molecules. Since a diastereoisomeric mixture gave rise to a very different, close-packed pattern, the formation of the open honeycomb network of the enantiopure compound was attributed to chiral self-recognition between the helically shaped motor units.[60]

It is observed, particularly on graphite surfaces, that alkyl chains on molecules often dominate the two-dimensional assembly. As a result of the specific orientation of the alkyl chains along the directing symmetry axes of the graphite lattice and their interdigitation with tails of adjacent molecules, together with a specific shape of the molecular core, nanoporous networks can be created solely based on van der Waals interactions. In this respect dehydrobenzo[12]annulenes (DABs; Figure 22 a) have proven to be excellent building blocks, because of their unique characteristics:[61,62] 1) the alkyl chains are oriented nearly perpendicular to the edge of a rhombic or triangular aromatic core, and 2) the distance between the alkyl chains on the same edge is 8.8 Å, which is ideal for interdigitation of alkyl chains. At the interface with graphite, 1,2,4-trichlorobenzene (TCB) form

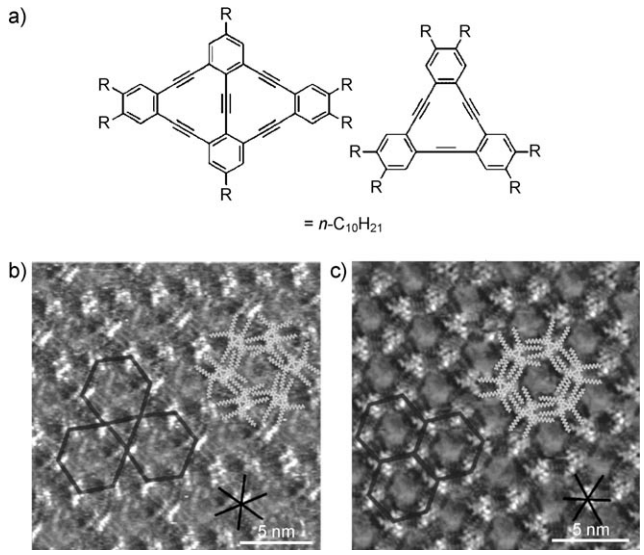

Figure 22. a) Molecular structure of DBAs with rhombic and triangular aromatic cores, respectively; b) STM image of the Kagomé network formed by the DBA with a rhombic core; the tentative model of molecular organization is superimposed; c) as (b) but of the honeycomb network formed by the DBA with the triangular core. Reprinted from Ref. [61] with permission from the American Chemical Society.

closely packed Kagomé or honeycomb porous networks (Figure 22b and c, respectively), with the interdigitating alkyl chains running along the three main symmetry axes of the graphite lattice. Similar networks based on the interdigitation of alkyl chains were realized using a stilbenoid compound with a 1,3,5-tristyrylbenzene conjugated core and peripheral decyloxy chains (TSB35; see Figure 27).[63]

4.1.4. ***Additional Factors Controlling Network Formation***

The self-assembly of molecules at a surface is a delicate process which is governed by a complex interplay between molecule–molecule and molecule–substrate interactions. Molecule–solvent and solvent–substrate interactions are also involved at a liquid–solid interface (see Section 2.2). It is far from trivial to understand and control all these factors, and thus be able to predict precisely the outcome of a two-dimensional self-assembly process. A first step to a rational assembly is through the careful design of the building blocks, for example, by careful choice of their molecular symmetry and flexibility and by attaching functional groups. Elegant examples of the influence that molecular symmetry can have on two-dimensional self-assembly are the DBAs described in Section 4.1.3, which generate different types of networks depending on the shape of the aromatic core of the molecules. In another example, in which both the molecular symmetry and the presence of certain functional groups are of importance, star-shaped oligofluorenes end-capped with various numbers of carboxylic acid groups were used (Figure 23a).[64] STM studies at the octanoic acid–graphite interface revealed that the two-dimensional self-assembled architectures of all these compounds are dominated by intermolecular hydrogen bonds, but vary depending on the number of carboxylic acid end groups. The molecule with one carboxylic acid group forms lamellae of dimers, the molecule with two carboxylic acid groups forms networks of zigzag chains, and the molecule with three carboxylic acid groups forms a highly porous honeycomb network with cavities with a diameter of 4.0 nm (Figure 23b–d).

In addition to molecular structure, the electronic properties and the structure of the underlying surface, which determines the type of interaction between the substrate and adsorbed molecules, can also have a key influence on the assembly of two-dimensional nanoporous networks. For example, the supramolecular cavity-containing rectangles shown in Figure 24a self-assemble at a graphite surface in an edge-on geometry in which their cavities are not exposed (Figure 24b,c).[65] In contrast, the same molecules self-assemble in a face-on geometry at a Au(111) surface in an EC-STM, with their cavities now oriented towards the STM tip (Figure 24d,e). The difference in orientation originates from a difference in the interaction strength between the surface and these particular molecules.

Although the nature of the molecule and the substrate will always be dominant factors in two-dimensional self-assembly processes, factors such as the solvent, surface coverage (under UHV conditions), and concentration (at the liquid–solid interface) can also play an important role, in particular when network polymorphs can exist, as shown earlier for TMA. In the case of TMA, the evolution of surface topology under UHV conditions depends exclusively on the surface coverage, a phenomenon which was also observed for other systems, such as hexaphenylbenzene (HPB) and 4,9-diaminoperylenequinone-3,10-diimine (DPDI).[66] The formation of different polymorphs of TMA at the liquid–solid interface was interpreted by stabilization of either TMA dimers or trimers by different solvents. Similar solvent-dependent polymorphism was revealed for the adsorption of BTB: for solvents with functional groups that are able to form hydrogen bonds with the solute, a rough dependence of the resulting two-dimensional structure on the dielectric constant was found.[48,50]

A strong solvent dependency was also observed for networks stabilized by van der Waals interactions. the four different solvents 1-phenyloctane, *n*-tetradecane, 1-octanoic acid, and TCB were tested for the networks based on DBA. STM studies revealed the presence of very complex polymorphs, which varied from highly porous networks to close-packed linear patterns. Sometimes clear coadsorption of solvent molecules was observed, which affected the shape of the assembled structure.[67] The solvent effect was discussed in terms of solubility, which may affect both the in-plane (diffusion) and out-of-plane (adsorption/desorption) mobility of the molecules at the interface, and in turn this may affect the speed of conversion from a kinetically trapped structure to a thermodynamically favored one. Certainly the viscosity of the solvent is expected to play a role by affecting the adsorption/desorption process.

Another important factor at the liquid–solid interface is the concentration of the solute, particularly when two-dimensional polymorphs with different packing density can be formed. It is surprising that it is only very recently that concentration effects have been systematically probed for physisorbed systems,[68] for example, the DBAs described in

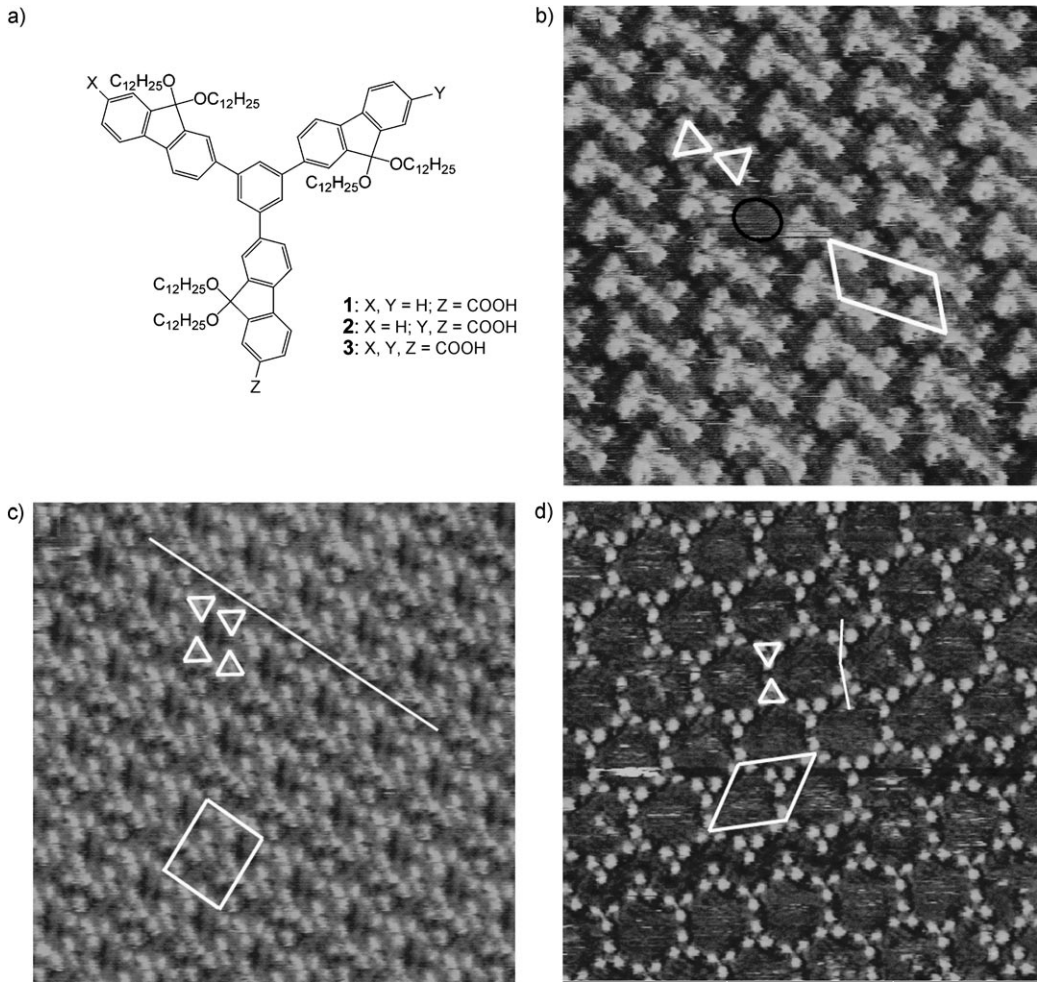

Figure 23. a) Molecular structure of the star-shaped oligofluorenes; b–d) STM images of the oligofluorenes with one, two, and three carboxylic acid groups, respectively. The bright triangles indicate the orientation of the aromatic cores in the assembly; white boxes: unit cells, dark circle: vacancy. Reprinted from Ref. [64] with permission from the American Chemical Society.

Section 4.1.3. DBAs form two-dimensional nanoporous networks at the graphite–TCB interface if their alkyl chains are shorter than 12 carbon atoms, while DBAs with longer chains preferentially self-assemble into close-packed linear arrays. However, the appearance and ratio of these polymorphs could be tuned by the concentration of the DBAs: regular honeycomb networks are formed at low concentrations, and densely packed linear networks at high concentrations (Figure 25).[69] By following this so-called "concentration-in-control" concept, nanoporous networks can be formed in which the pore size is determined by the length of the alkyl chains and can be tuned from 2.9 to 5.4 nm with increments of about 0.4 nm. The influence of the concentration on the ratio of the polymorphs was modeled assuming that the adsorption/desorption equilibrium is under thermodynamic control. It was shown that the solute concentration is directly related to the difference in stability between the linear and the honeycomb polymorphs and their respective molecular densities, and were in accord with the proposed model. This dilution principle has already been put into context with the concentration dependence of surface aggregates produced in a vacuum.[66c]

The concentration-in-control concept is also applicable to the assembly of multicomponent networks.[70] Alteration of concentrations of the two different carboxylic acids BTB and TMA in binary solutions results in the formation of six nondensely packed porous network phases with different structures and stoichiometries. All these patterns are stabilized by pairwise hydrogen bonding between carboxylic acid moieties, but they differ in the number of cavities. Phase transitions between the monolayer structures can be achieved by in situ dilution.

Lowering the concentration while keeping the ratio of both species constant favors the formation of networks with lower surface coverage, similar to that observed for the single-component DBA networks.

4.2. Properties of Nanoporous Networks

4.2.1. Engineering the Size and Symmetry of the Cavities

For many applications, such as the immobilization and isolation of functional objects, it is important to obtain two-dimensional porous networks which have a tunable cavity size and periodicity. In Section 4.1 it was demonstrated that this can be accomplished by varying the spacers between hydrogen-bonding carboxylic acid functional groups, the ligand size in MOFs, or the length of the interdigitating alkyl chains. Large pore sizes were obtained, for example, in honeycomb networks composed of cobalt carbonitrile building blocks (5.7 nm)[71] and of DBAs with C_{30} alkyl chains. In the latter network, pores with a diameter of 7.5 nm and a cavity fraction of 0.58 were achieved, which makes it the most open network reported so far.[72]

Another strategy has recently been reported: by varying the number and size of bulky substituents attached to porphyrin-based building blocks, not only could the dimensions of the surface assembly (one-dimensional wires or two-dimensional porous networks, as well as the pore-to-pore distance) be tuned, but also new assembly motifs could be induced. Porphyrin derivatives **4**–**6** self-assemble into porous networks with *p*3 symmetry on a Cu(111) surface (Figure 26).[73] The distances between the pores increase

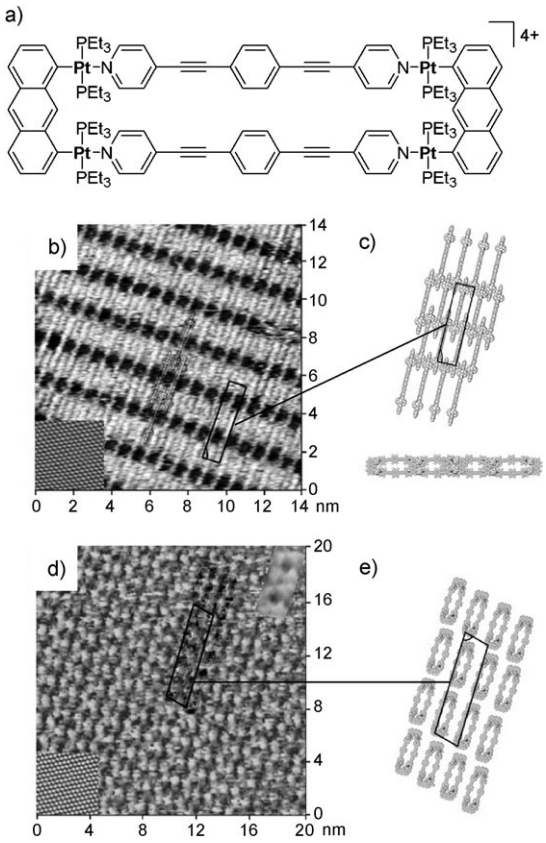

Figure 24. a) Molecular structure of a supramolecular rectangle; b) STM image of a network of the rectangles on graphite (inset: STM image of graphite); c) molecular models (top and side view) illustrating the "edge-on" orientation of the rectangles on graphite; d) EC STM image of a network of the rectangles at an interface of Au(111) and a 0.1 M $HClO_4$ solution in water (inset: graphite lattice underneath the monolayer); e) molecular model illustrating the face-on orientation of the rectangles on Au(111). Reprinted from Ref. [65] with permission from the National Academy of Sciences, USA.

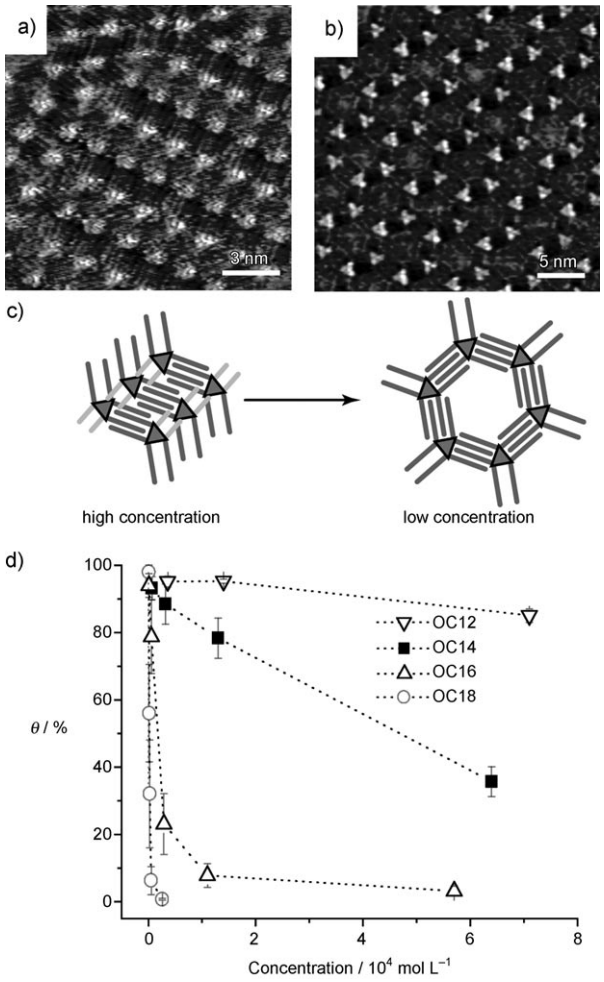

Figure 25. a, b) STM images of linear and honeycomb networks formed by a DBA with hexadecyloxy chains at the TCB–graphite interface at high and low concentrations, respectively; c) schematic illustration of the "concentration-in-control" concept; d) concentration dependence of the surface coverage of honeycomb networks (θ) of DBAs with different alkoxy chains; OC*n*: alkoxy chains with *n* carbon atoms. Reprinted from Ref. [68].

from (30.9 ± 0.2) Å for **4** and (33.5 ± 1.2) Å for **5** to (48.0 ± 1.4) Å for **6**. Besides the typical supramolecular synthons A and B (Figure 26b), which were initially observed in three-dimensional crystals, two new synthons were discovered. The porous network formed by **4** is stabilized by three C≡N···H–C hydrogen bonds between the 4-cyanophenyl groups and the β-hydrogen atoms of three adjacent porphyrins with formation of a cyclic arrangement (see B). The stabilizing supramolecular synthon for the network formed by porphyrin **6** is depicted as D. In this nonsymmetric trimeric motif, each cyanophenyl substituent acts both as a hydrogen-bond donor and as an acceptor. The change in the structure of the supramolecular synthon upon going from **4** to **6** via **5** was attributed to the increased steric hindrance between the molecules as the number and size of the alkoxy chains increased, which prevent adjacent molecules from approaching each other.

4.2.2. ***Host–Guest Aggregates***

The most important property and application of two-dimensional nanoporous networks so far is the accommodation of guest molecules inside the cavities. The regularity of the network offers the possibility to arrange functional molecules and clusters of metals or semiconductors in a repetitive and spatially ordered arrangement. As such, host–guest networks can also serve as an ideal matrix to study the dynamics of guest binding, diffusion, and manipulation by STM.

The hexagonal cavities in the honeycomb network formed by TMA are highly robust and stable enough to endure scanning by an STM tip, and they thus serve as an ideal platform to study single-molecule dynamics and the manipulation of bound guest molecules.[50] In this way, C_{60} guest molecules bound in the cavities of the TMA network at a liquid–solid interface could, for example, be laterally manip-

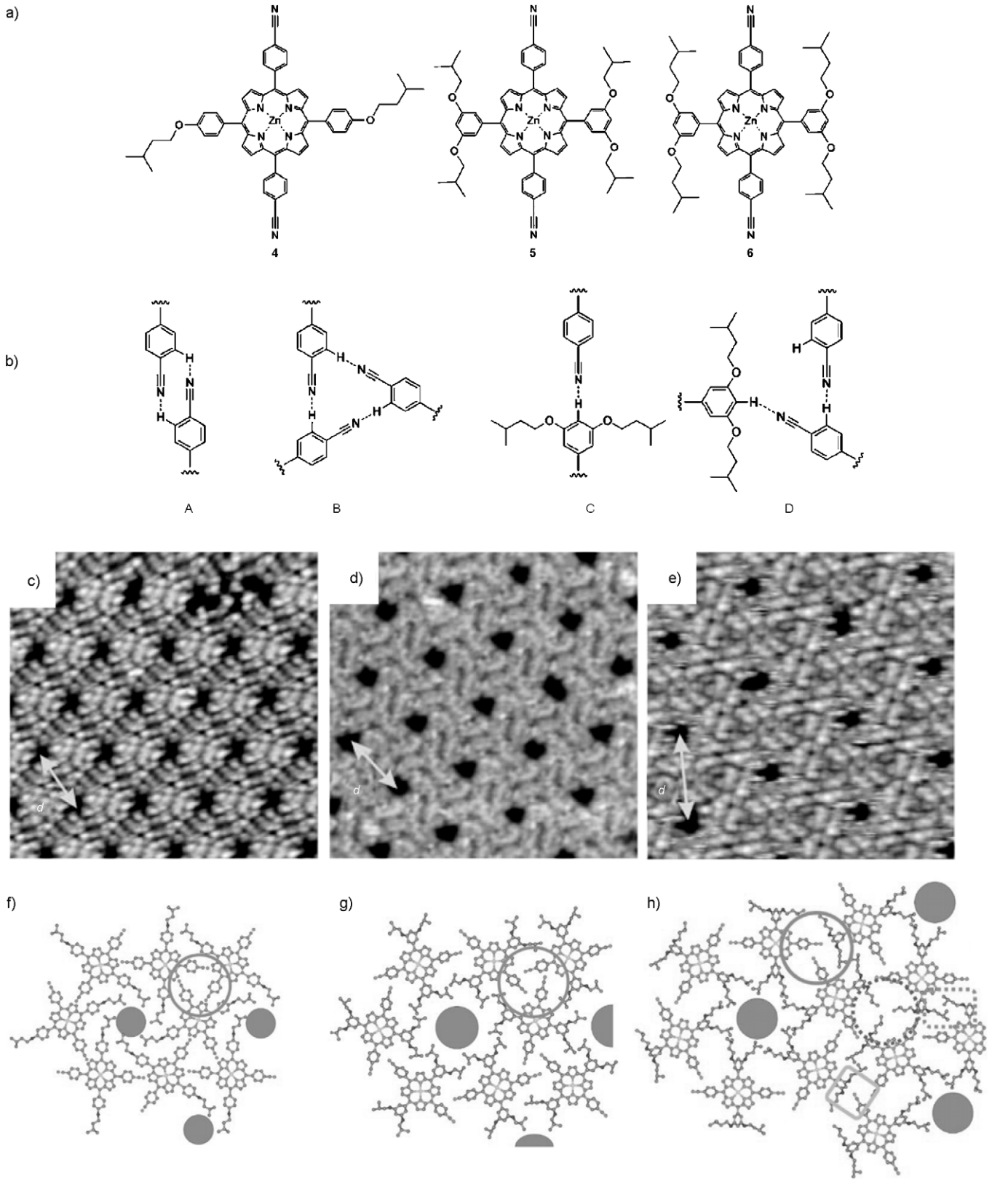

Figure 26. a) Chemical structures of the three porphyrin derivatives **4**–**6**; b) supramolecular building blocks formed by two (A) or three (B) interacting 4-cyanophenyl groups, as well as those formed by the interaction of the 4-cyanophenyl group with a 3,5-alkoxyphyenyl group (C and D). STM images (c–e, all 15×15 nm^2) and corresponding tentative models (f–h) of the open networks formed by porphyrin derivatives **4**–**6**, respectively, at a coverage close to one monolayer; d = lattice constant. Reprinted from Ref. [72].

ulated in a well-defined fashion by the STM tip simply by lowering the tunneling current.[74] In another example, the well-defined alignment of guest molecules in a nanoporous network also allowed real-time investigation of the dynamics of guest molecules and the interactions between them at the single-molecule level. Guest molecules such as coronene and hexabenzocoronene (HBC) could be hosted in a network composed of TSB35 molecules (Figure 27).[63] Investigation of the size- and shape-dependent dynamics of these guests within the network showed that HBC remained immobilized as a result of its commensurate size, while coronene underwent fast rotational and translational diffusion within the network. Histograms of the residence time of the guest within a cavity at different temperatures gave insight into the diffusion mechanism. The temperature dependence revealed that guest diffusion proceeded through thermally activated channeling between single-molecule surface cavities.

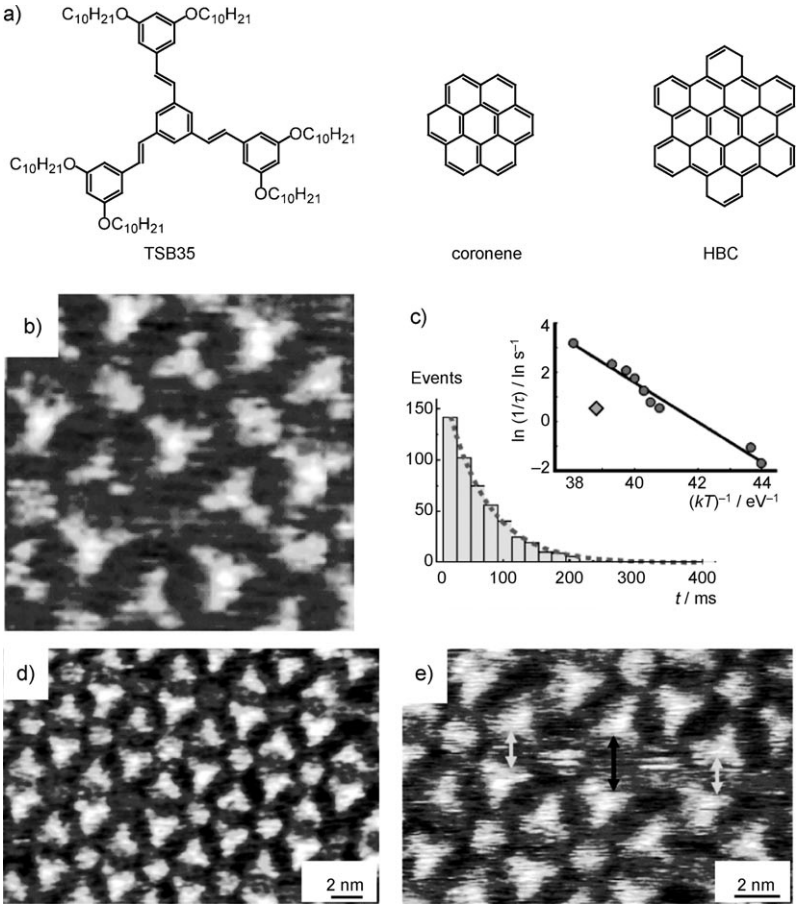

Figure 27. a) Molecular structures of TSB35, coronene, and HBC. b) STM image (11×11 nm^2) of the network formed by the TSB35 matrix filled with coronene guests. c) Histogram representing the decay of the presence of a coronene guest in a cavity, as derived from a series of successive images. The inset shows the temperature dependence of the decay constant at the liquid–solid interface (circles) in comparison to that measured under a vacuum at room temperature (diamond). The solid line represents an Arrhenius line with an energy barrier of (0.81 ± 0.05) eV. d) STM image of an incompletely filled matrix with substoichiometric concentrations of HBC. e) STM image showing a defect where the distance between two neighboring TSB35 molecules is increased by 50%, and indicating the motion of a HBC guest between the two adjacent cavities (black and white arrows). Reprinted from Ref. [63b] as well as from Ref. [63a] with permission from the American Chemical Society).

Porphyrin derivatives with similar structures as shown in Figure 26 (Section 4.2.1) can form well-ordered porous networks on a Ag(111) surface. Subsequent co-deposition of C_{60} molecules results in the selective inclusion of the fullerenes within the preformed cavities. Interestingly, a distinct interaction between fullerene guests over distances longer than their van der Waals radii was observed, as was evidenced by the presence of long fullerene chains and 2D arrays.[75] The nature of the long-range interaction was investigated further by comparing the diffusion behaviors of C_{60} and C_{70}. A systematic investigation of the hopping rates as a function of fullerene coverage was performed and the data were interpreted in a quasichemical approach, which describes a two-dimensional lattice gas with interacting particles. The hopping rate of C_{60} increases from a coverage of zero to 0.3 monolayer (ML), followed by a strong decrease at higher values. In contrast, the hopping rate of C_{70} starts decreasing strongly right away, and rapidly reaches a value that is about two orders of magnitude lower. According to the quasichemical approach, the pronounced decrease in the hopping rate of C_{70} is caused by the presence of a distinct attractive interaction between nearest neighbor fullerene molecules. In the case of C_{60}, a repulsive nearest neighbor interaction is effective at low coverage, which decreases with increasing coverage and becomes attractive at high coverage (> 0.45 ML). However, the microscopic mechanisms behind the long-range interactions remain unclear.

If the network has cavities that are large enough, then not only can single guests be hosted but so can guest clusters. In the MOF formed by Fe atoms and TDA ligands (see Section 4.1.2), added C_{60} molecules were in some cases bound as dimers or even trimers in a cavity.[57] In the nanoporous network formed by melamine and PTCDI on a Si(111) surface under UHV conditions (pore diameter: nearly 3 nm), hexagonally arranged heptameric clusters of C_{60} clusters are hosted in a compact fashion when the guest molecules were sublimed onto the preformed open network (Figure 28 a).[56] Clusters formed in different pores are aligned and all oriented parallel to the principal axes of the underlying silicon surface.

Heteromolecular clusters composed of six isophthalic acid molecules and one coronene guest could be prepared at a liquid–solid interface by utilizing the perfect commensurability between a coronene guest and the pores found in a TMA honeycomb network. This heterocluster with a well-defined composition and symmetry could subsequently be accommodated in the cavities of a network of a DBA with decyloxy

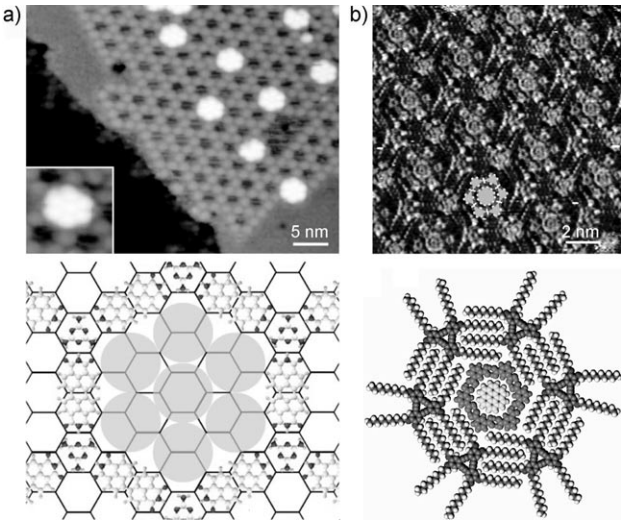

Figure 28. a) STM image of heptameric clusters of C_{60} trapped within the hexagonal cavities of a PTCDI–melamine network; the inset shows a high-resolution image of an individual cluster; b) STM image of the coronene–isophthalic acid heterocluster trapped in a network formed by a DBA with decyloxy chains; a model of the heterocluster is superimposed on the image. Corresponding models are shown below the images. Reprinted from Refs. [56] and [75] with permission from the Nature Publishing Group and the American Chemical Society.

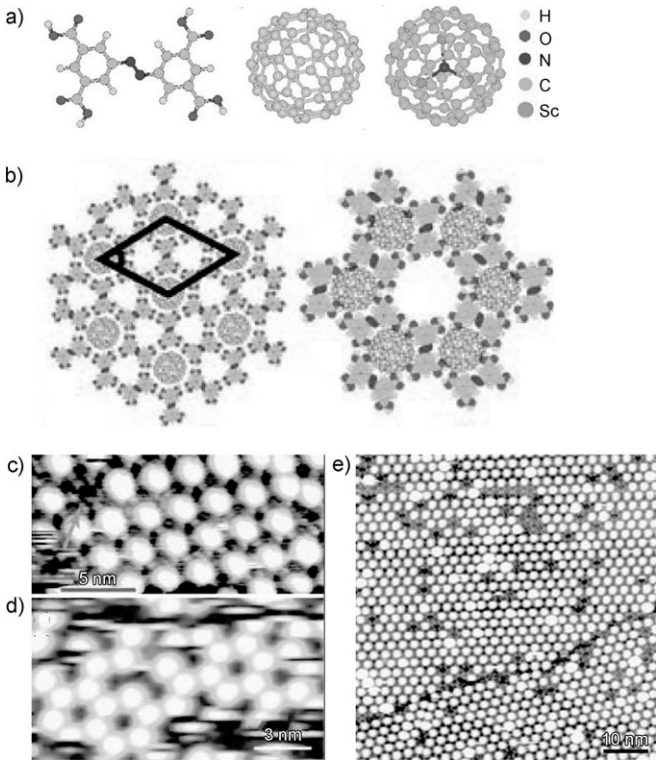

Figure 29. a) Molecular structure of the azobenzene derivative with four acid groups as well as C_{60} and $Sc_3N@C_{80}$ (from left to right); b) models of the Kagomé network with the C_{60} guest molecules trapped in the hexagonal (left) and triangular (right) cavities; c) STM image of the host–guest structure of the Kagomé network and C_{60} with the guest molecules trapped in the hexagonal cavities; d) as (c), but with the guests trapped in the triangular cavities; e) as (c), but of the network and $Sc_3N@C_{80}$ with the guests trapped exclusively in the hexagonal cavities. Reprinted from Ref. [76].

alkyl chains (Figure 28b).[76] These developments pave the way for new applications, such as the use of nanoporous networks as nanoreactors to create oligomers with a well-defined size, symmetry, and composition by established chemical procedures.

At the 1-heptanoic–graphite interface the azobenzene tetraacid derivative shown in Figure 29a forms stable Kagomé networks with pores of different size and symmetry aligned in a well-defined way. It can be expected that adding specific guests to such a network might result in them displaying a site selectivity, depending on the size and symmetry commensurability of the guest and the cavities in the network. STM studies showed that when C_{60} was added to the network, two coexisting self-assembled structures were observed, differing by the adsorption sites of the guests—either in the triangular or in the hexagonal sites (Figure 29b–d).[77] This finding indicates that adsorption of C_{60} in these sites is energetically equally favorable, which was confirmed by theoretical calculations. Interestingly, no domains were observed in which C_{60} molecules occupied both types of cavities, possibly because of repulsive interactions or by modulation of the electronic characteristics of the host matrix by the adsorption of the guests. However, C_{80} or $Sc_3N@C_{80}$, both larger than C_{60}, were observed to occupy the larger hexagonal pores exclusively (Figure 29e). The size and geometry commensurability of the guests with these cavities is believed to play a substantial role in the observed site selectivity, again confirmed by theoretical calculations.

Besides serving as a platform for the study of dynamics[63] and manipulation of single molecules,[78] well-ordered nanoporous networks can also serve as a platform for the preparation of spatially highly ordered and independently addressable single molecules, for example, supramolecular multiposition rotary devices. The zinc porphyrin derivative shown in Figure 30a self-assembles at a Cu(111) surface into a regular nanoporous network as a result of weak hydrogen bonding between protons on the phenyl rings and the cyano residues.[79] The arrangement of the porphyrin rings around the pores is chiral, and both types of homochiral domains were observed at the surface. Interestingly, the molecules could be trapped on top of the pores, such that they made no contact with the substrate; they can then rotate freely between six possible orientations, which makes it a single-molecule rotator. The rotation speed was found to depend on the temperature, and switching events of individual guests between different stable orientations could be monitored by STM around 112 K. Analysis of successive STM images taken at temperatures between 112 and 116 K allowed the switching activation energy to be estimated as (0.24 ± 0.08) eV (Figure 30d). An even more interesting observation was that the individual guest molecules could be selectively addressed and switched by the STM tip at 77 K, a temperature where no thermally induced switching occurs. Single switching events could be triggered with molecular precision by placing the

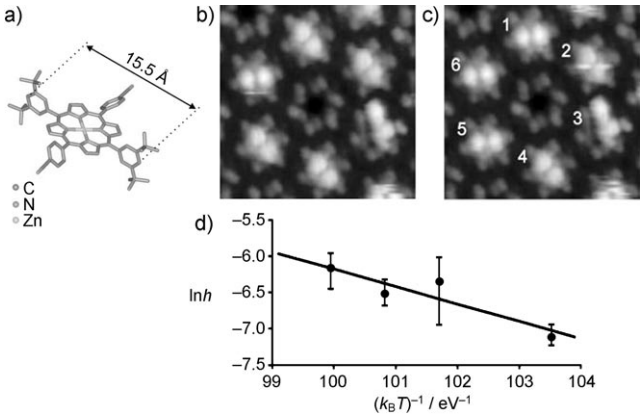

Figure 30. a) Molecular structure of the zinc porphyrin derivative; b, c) sequential STM images taken at 112 K of the porous network formed by this compound (scan size: 7.4×7.4 nm^2). Some of the pores are filled by guest molecules (1–6), which appear dumbbell-shaped and which can be switched over time to a different position (see the orientations of 1 and 5); d) Arrhenius plot for the determination of the activation energy needed to switch a guest molecule between two neighboring positions. Reprinted from Ref. [78].

STM tip above a guest molecule, and applying a short pulse, leaving neighboring guests unaffected.

A similar rotary device was realized by inclusion of zinc octaethylporphyrin (OEP) into a prefabricated hexagonal network generated by thermal dehydrogenation of 4,9-diaminoperylenequinone-3,10-diimine (DPDI) on a Cu(111) surface.[80] The energy barrier of this molecular rotor in the confined space of the surface network was determined to be (0.17 ± 0.03) eV.

4.2.3. *Network Functionalization*

In principle, two-dimensional nanoporous networks can be further functionalized by attaching reactive groups to the rims or vertices of the constituting molecules. In this way, guest binding by templating may be combined with specific molecular recognition interactions. As was discussed in Section 4.1.2, the MOF formed by TMLA on a Cu(100) surface under UHV conditions contains organic ligands in which one carboxylic acid group is not involved in metal–ligand coordination, but points towards the interior of the pore and appears to have a profound influence on the interaction with C_{60} guests in the sense that their binding stability was increased.[57]

Very recently it was demonstrated that modification of the building blocks of porous networks with functional groups could also lead to completely new self-assembled structures. In the PTCDI/melamine networks described in Section 4.1.1 the PTCDI component was replaced by derivatives containing either bromine or propylthio substituents at the perylene core (Figure 31 a).[81] STM studies on a Ag/Si(111) surface under UHV conditions revealed that the introduction of the bromine substituents had only a small effect on the structure of the homomolecular network. The deposition of melamine onto a sub-monolayer of Br_2-PTCDI showed that the bromine substituents even favor the formation of the heteromolecular honeycomb network compared to the standard PTCDI–melamine network. In addition, the formation of heptameric clusters of guest molecules in the cavities upon the addition of C_{60} highlighted the similarity in host–guest behavior of the two networks (Figure 31 d).

In contrast, the attachment of propylthio groups gave a significantly different homomolecular network with a smaller periodicity (28.3 versus 35 Å) compared to the network formed by PTCDI. Attractive C–H···O hydrogen-bonding interactions between the propylthio chains and oxygen atoms on a neighboring molecule is proposed to be responsible for the change in the di(propylthio)-PTCDI network (Figure 31 b,c). After deposition of melamine, similar heteromolecular honeycomb networks as observed with PTCDI and Br_2-PTCDI were formed, but which exhibited totally different host–guest properties. Instead of clusters of C_{60} guests, C_{60} monomers were only observed irregularly inside the pores or on top of the network (Figure 31 e). The inability of the pores to bind clusters of guests was proposed to be caused by the bulky propylthio chains inhibiting interactions between C_{60} and the underlying surface.

4.2.4. *Combining Physisorption with Chemisorption: Hybrid Nanoporous Networks*

Self-assembled monolayers (SAMs), typically thiols chemisorbed on metal surfaces, are widely used to tailor chemical and physical properties of interfaces and to generate patterned surfaces. Combining the noncovalent self-assembly of porous networks with SAMs provides a powerful method, with the former process providing nanometer-scale precision and the latter offering a wide variety of functionalization possibilities. For this purpose the melamine–PTCDI network was prepared by a solution-based assembly on a gold surface, which allows subsequent processing with SAMs of thiols and related compounds.[82] The coadsorption of PTCDI and melamine from dimethylformamide resulted in the formation of a regular honeycomb network on Au(111) with a periodicity of 35 Å, identical to the network formed under UHV conditions (Figure 32 a). STM revealed that the network was capable of serving as a template for the formation of SAMs of three types of thiols that differed in the stability of their monolayers. After thiol adsorption, the honeycomb network remained intact, and its structural rigidity allowed molecular resolution of the internal SAMs of adamantane thiol (Figure 32 c). The SAM–network hybrid structures were stable in a liquid environment and could be processed further by electrochemically depositing copper between the thiols and the Au(111) surface (Figure 32 d,e). Cross-sectional analyses of processed and unaltered areas proved that Cu was only inserted between the thiols and the substrate and not between the PTCDI network and the substrate. Such a combination of physisorbed noncovalent networks with chemisorbed SAMs offers considerable design flexibility, with the network providing a well-defined confinement of structures within the substrate plane, and the SAM permitting orthogonal modification of the surface.

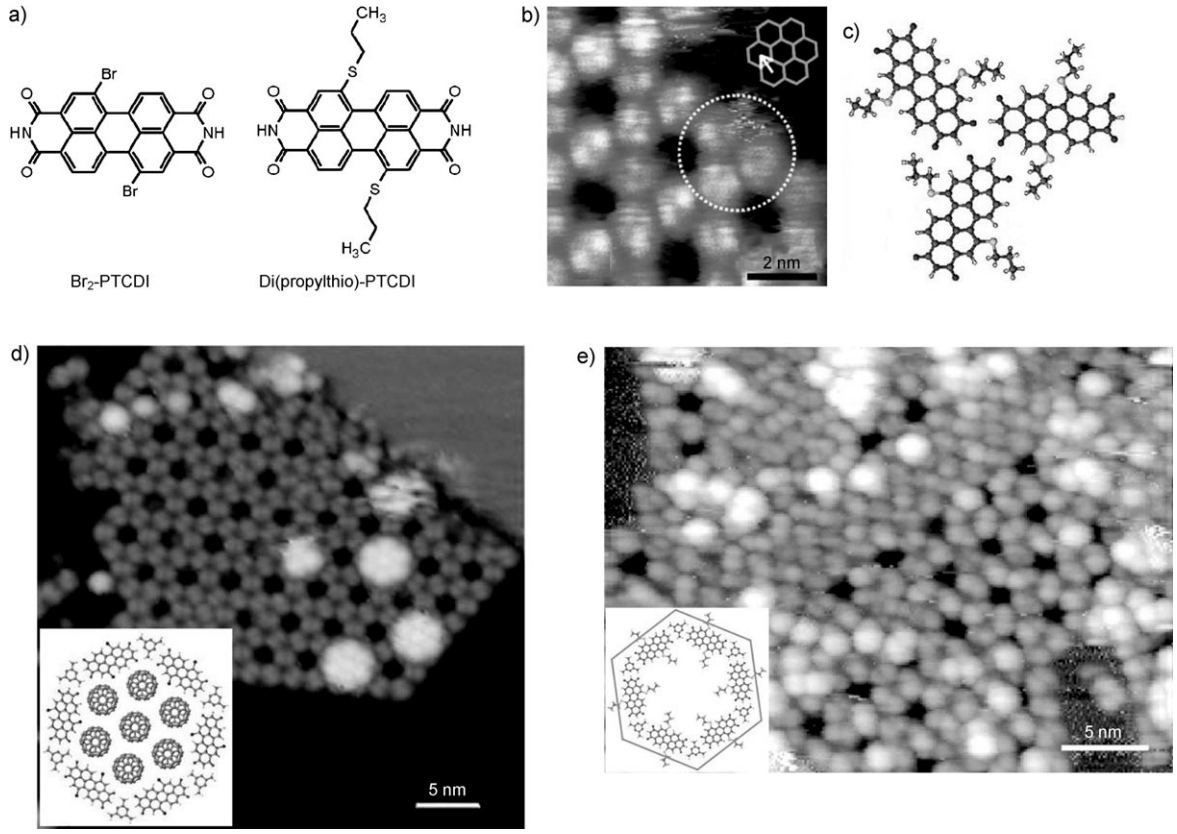

Figure 31. a) Molecular structure of Br_2-PTCDI and di(propylthio)-PTCDI. b) STM image of a homomolecular network formed by di(propylthio)-PTCDI. A trimer node is highlighted by a dashed white circle and the surface reconstruction of the Ag/Si(111) by a hexagonal mesh; arrow: [11$\bar{2}$] direction of the surface. c) Molecular model proposed for the trimer node. d) STM image showing three captured C_{60} heptamers within the cavities of a Br_2-PTCDI-melamine network; inset: molecular model. e) STM image showing the disordered structure after deposition of C_{60} onto a di(propylthio)-PTCDI-melamine network; inset: a model of the network in which the cavity is partially occupied by the propylthio substituents. Reprinted from Ref. [80].

5. Chemical Reactivity on Surfaces: Along New Pathways

The previous sections have shown that nowadays a wealth of two-dimensional self-assembled nanostructures can be constructed on surfaces by following bottom-up strategies that make use of elements from the repertoire of supramolecular chemistry. STM has proven to be a unique tool to characterize these nanostructures at the highest level possible, that is, by imaging single atoms and molecules. An even more appealing possibility is to use STM to visualize dynamic phenomena, in particular reactivity, in the self-assembled nanostructures in real time and space.[83] Chemical reactions are conventionally studied by ensemble techniques, for example, NMR and fluorescence spectroscopy, but these share the limitation that only average behavior is measured and information at the single-molecule level remains hidden. Only recently, fluorescence microscopy has been applied to monitor, by single turnover counting, chemical reactions carried out on crystal faces,[84] by enzymes,[85] on nanoparticles,[86] and during the formation of metal–ligand complexes.[87] With the invention of STM it has become possible to really visualize chemical reactions at the atomic level. Amongst others,[88] Nobel laureate Gerhard Ertl was one of the pioneers to apply scanning probe techniques to study molecular mechanisms of elementary reactions at surfaces in detail,[89] such as the catalytic synthesis of ammonia over iron and the oxidation of carbon monoxide over palladium. A variety of other simple reactions involving single-molecule oxidations[90] and the modification of chemical bonds, such as rotation,[91] diffusion,[92] dissociation,[93] isomerization,[94] and chemical bond formation,[95] were later investigated by STM. In recent years, however, a shift of attention towards the study of reactions between much larger organic molecules has become apparent, in particular in the area of covalent coupling reactions under UHV conditions, and even more recently, in the area of reactions that occur at the liquid–solid interface, which is the typical research area of the chemistry and biology disciplines. This section will focus on the newest developments in the latter two areas.

5.1. Reactivity Under UHV Conditions

In 2000 Hla and co-workers published a seminal paper in which they described the coupling of two iodobenzene molecules to give a biphenyl molecule at low temperatures under UHV conditions.[113] All the steps of this Ullmann-type

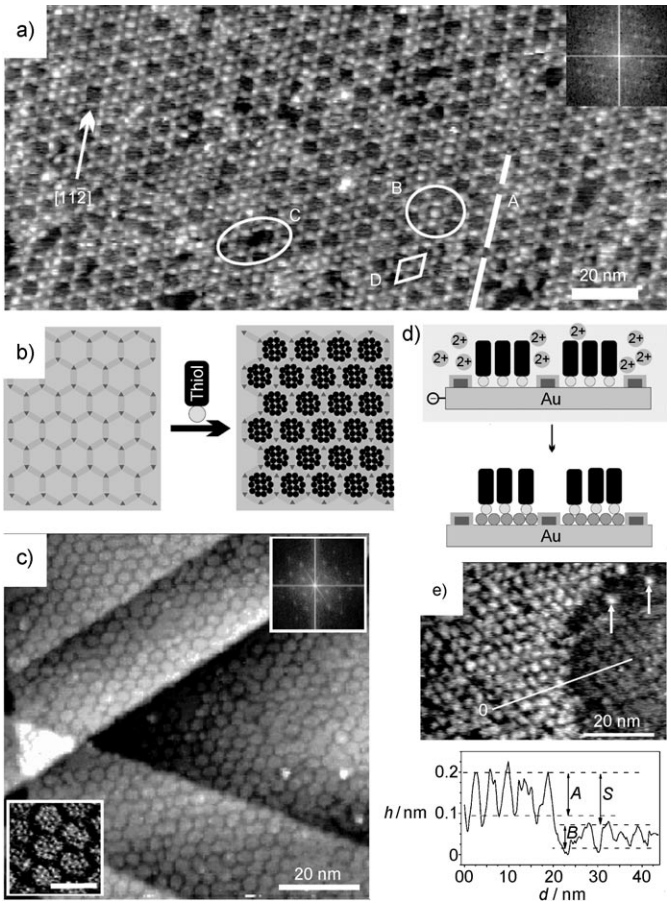

Figure 32. a) STM image of a PTCDI–melamine network formed by solution deposition on a Au(111) surface; the dashed line A marks a fault line; circles B and C mark a pore filled with a PTCDI molecule and a missing PTCDI molecule, respectively; D: 35 Å period of the honeycomb lattice; inset: Fourier transformation highlighting the regularity of the network. b) Schematic representation of the filling of the cavities of the PTCDI–melamine network by thiols. c) STM image of the hybrid structure on Au(111), with the network filled by adamantane thiol; inset bottom left: an image with molecular resolution of the thiols inside the cavities (scale bar: 5 nm); inset top right: Fourier transform. d) Schematic representation of the electrochemical deposition of Cu in pores of the network at the thiol–gold interface. e) STM image of a sample taken in an ambient atmosphere after partial electrochemical deposition of Cu; the arrows mark isolated pores where Cu deposition has occurred; bottom: the height profile along the line given in the image; *A*, *B*, *S*: height differences of 1.15, 0.5, and 1.3 Å, respectively. Reprinted from Ref. [82] with permission from the Nature Publishing Group.

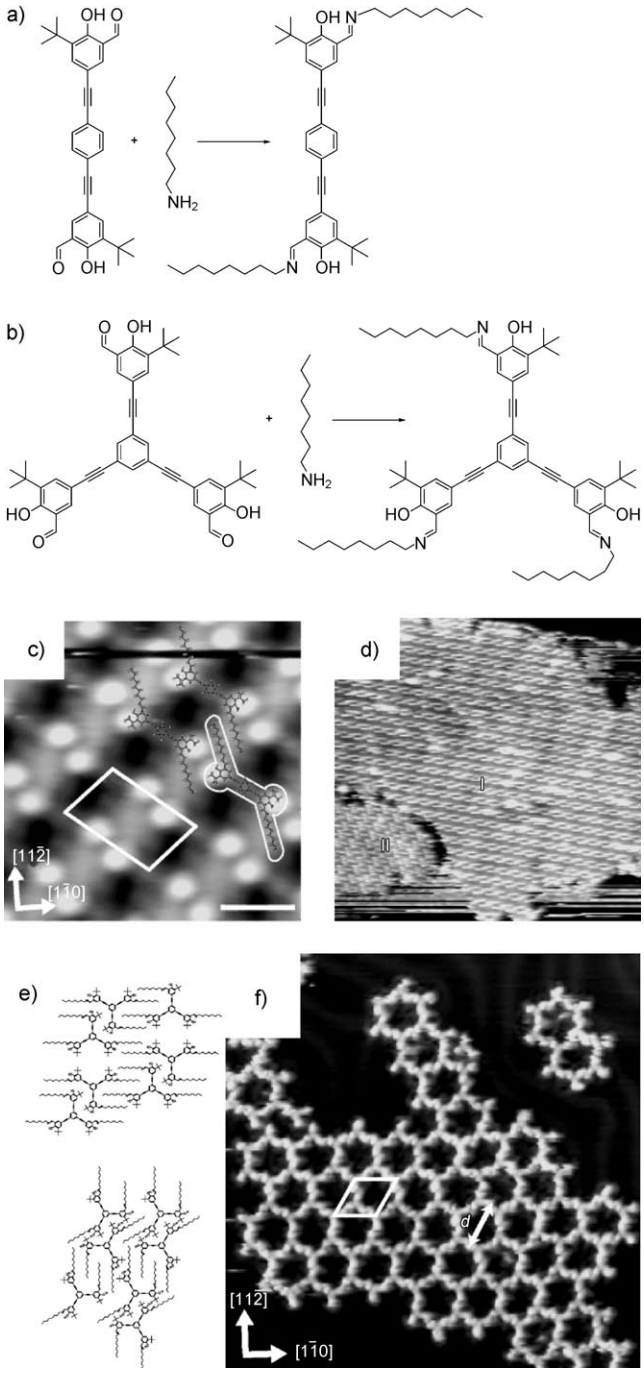

Figure 33. a) Condensation reaction between the dialdehyde and *n*-octylamine; b) as (a), but between the trialdehyde and *n*-octylamine; c) STM image of the self-assembled diimine product formed in situ at the surface; scale bar: 2 nm; white box: unit cell; highlighted molecular structure: single molecule of diimine product; d) STM image (85×85 nm^2) of self-assembled tightly packed triimines formed in situ at the surface at low temperature and high amine flux; e) molecular models of the two types of tightly packed phases (I and II) in the STM image in (d); f) STM image (40×40 nm^2) of the porous network formed by triimines formed in situ at the surface at high temperature and low amine flux; white box: unit cell, *d*: pore diameter. Reprinted from Ref. [97] with permission from the American Chemical Society.

coupling, carried out on the step edge of a Cu(111) surface, could be induced by the STM tip. In recent years a remarkable revival of two- or multicomponent coupling reactions has occurred, mainly with the aim to covalently connect large numbers of molecules to form robust two-dimensional networks over extended dimensions.[96]

Bisimines, for example, can be formed in situ at a Au(111) surface under UHV conditions by coadsorbing a bis(hydroxybenzaldehyde) and *n*-octylamine at room temperature (Figure 33a).[97] The identity of the condensation product was confirmed by comparing the STM images (Figure 33c) with

those of the product synthesized ex situ and by near-edge X-ray absorption fine structure (NEXAFS) studies. The fact that this reaction succeeds under UHV conditions was surprising, because imine formation in solution involves dehydration of a hemiaminal intermediate, which is a reaction catalyzed by the solvent acting as a combined proton donor/acceptor. DFT calculations predicted that in the absence of solvent the phenoxy group of the aldehyde, which is in proximity to the reactive site, can serve as an internal catalyst for dehydration. However, it was also realized that the underlying Au(111) surface might have a pronounced influence, for example, by lowering the energy barriers involved with the coupling reaction.

The combination of self-assembly and reactivity at the surface was further investigated by condensing *n*-octylamine with a star-shaped trialdehyde (Figure 33b).[98] It appeared to be possible with these components to control the final two-dimensional structure of the monolayer after reaction, depending on the reaction/assembly conditions. At low substrate temperature (170 K) and a high amine flux, kinetically formed close-packed networks were observed which exhibit the structural characteristics of the conformationally ordered trialdehyde reactant and after reaction are stabilized by attractive van der Waals interactions (Figure 33d,e). In contrast, open porous networks with a high degree of conformational disorder were formed at high substrate temperature (300 K) and a low amine flux, (Figure 33f). In this case, the higher substrate temperature destabilizes the adsorption of the trialdehydes which are allowed to diffuse freely over the substrate while reacting with the amines. Eventually, conformationally disordered hexagonal structures are entropically favored. Interestingly, the ex situ synthesized triimine product formed completely different networks when it was adsorbed on the surface, thus highlighting the possibility of on-surface synthesis to create unique new two-dimensional nanostructures.

In follow-up studies, the same condensation reaction was applied to create in situ polymeric networks by treating the trialdehyde with 1,6-diaminohexane.[99] The order and connectivity in these networks could be tuned by varying the conditions used to prepare the sample. When a cold surface ($T = 120$–160 K) supporting the trialdehyde was exposed to a

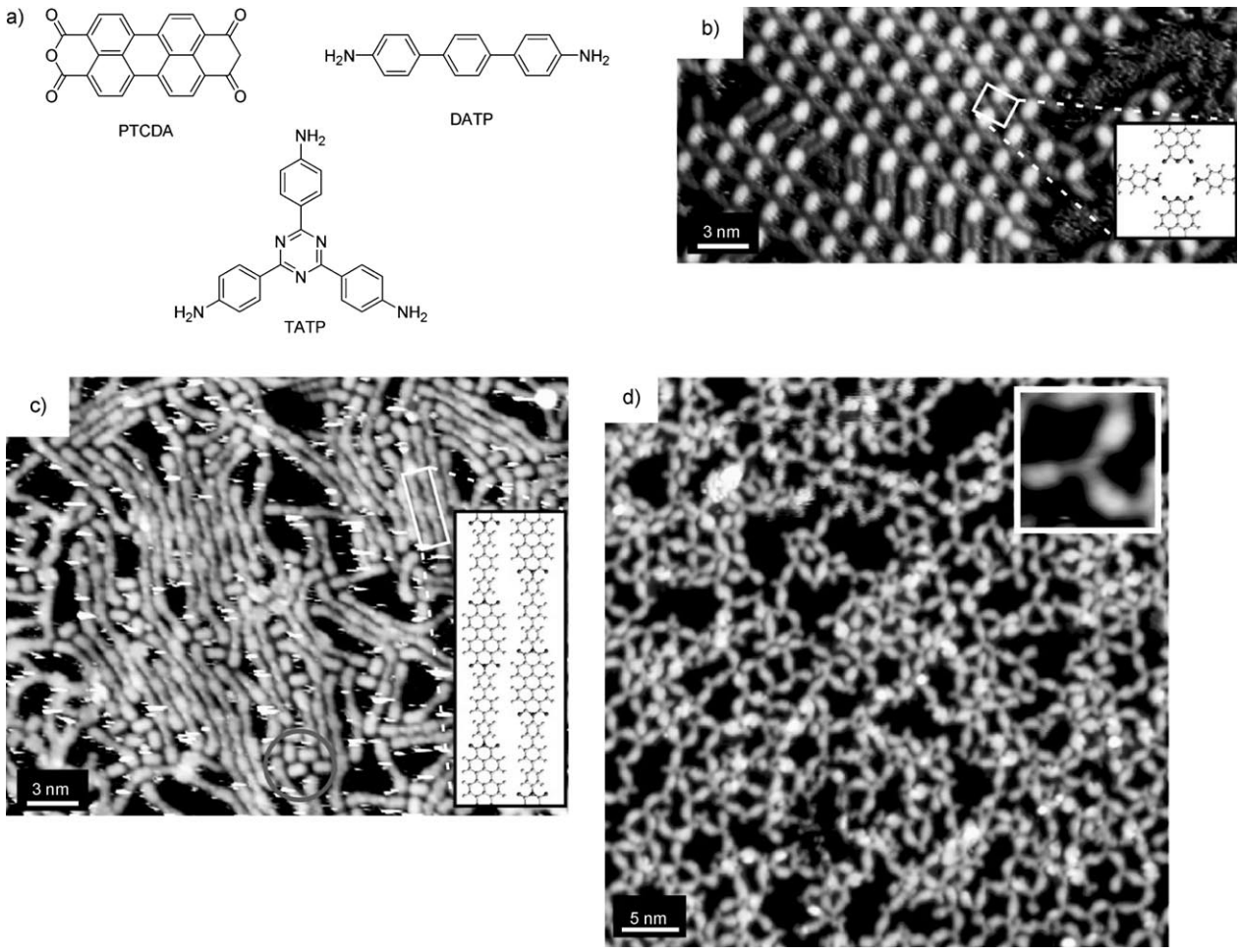

Figure 34. a) Molecular structures of PTCDA, DATP, and TATP; b) STM image of a two-dimensional hydrogen-bonded network of PTCDA and DATP on a Au(111) surface under UHV conditions; inset: arrangement of the molecules; c) STM image of parallel strands of agglomerated oligoimides after annealing the sample at 570 K; inset: arrangement of the molecules; d) STM image of a porous polyimide network obtained after annealing a 2:3 mixture of TAPT and PTCDA; inset: magnification. Reprinted from Ref. [99] with permission from the American Chemical Society.

vapor of the diamine, bicomponent multilayers were formed which were induced to react by annealing at 400–450 K. The high concentration of the diamines, which make them readily available for reaction, causes them to saturate the trialdehydes, and as a result oligomeric structures with low connectivity are formed. In contrast, oversaturation was prevented when a heated sample ($T = 400$ K) of the trialdehyde was exposed to a much lower pressure of diamine vapor, and extended polymer networks with high connectivity were formed.

Besides imines, imides can also be synthesized readily by a surface-confined reaction. When equal amounts of 3,4,9,10-perylenetetracarboxylic dianhydride (PTCDA) and 4,4′-diamino-*p*-terphenyl (DATP) were deposited at a Au(111) surface under UHV conditions (Figure 34a), STM images revealed the presence of a rectangular network of the two components, which interact through hydrogen bonds (Figure 34b).[100] Annealing at 570 K initiated an imidization condensation reaction that resulted in the formation of long parallel strands consisting of agglomerated polyimide oligomers (Figure 34c). The chain termini of these oligomers can be controlled to be either a PTCDA or DATP molecule by depositing one of these oligomers in excess. In addition to linear strands, branched networks can also be created by using, instead of DATP, 2,4,6-tris(4-aminophenyl)-1,3,5-triazine (TATP). A highly porous but irregular network exhibiting an extensive two-dimensional connectivity was obtained by treating these PTCDA and TATP components in a similar way (Figure 34d).

Another route to the in situ preparation of porous networks at a surface makes use of boronate-based reactions. The dehydration of 1,4-benzenediboronic acid (BDBA) in an intermolecular reaction at a Ag(111) surface under UHV conditions gave trimeric boroxines which organized into a hexagonal porous network with a pore size of 1.5 nm (Figure 35a).[101] The pore size could be increased by carrying out a heteromolecular coupling reaction, namely by esterification of BDBA with a hexahydroxytriphenylene (HHTP, Figure 35b). The resulting network consisted mainly of hexagons with a pore size of almost 3 nm. In the latter reaction, homopolymerization of BDBA was prevented by first depositing a monolayer of HHTP at the surface, followed by co-deposition of the two components. Excess water and HHTP were then removed by annealing. Both the dehydration and esterification reactions readily proceeded at room temperature, which implies that the activation temperature is lower than that. The robustness of the covalent networks was demonstrated by the fact that they survived annealing at 750 K for at least 5 minutes.

By confining potentially reactive molecules at a surface, it is in some cases possible to study reactions which do not easily take place in solution. An example of such a reaction is the oligomerization of 1,3,8,10-tetraazaperopyrenes (TAPP), which occurs via a carbene intermediate (Figure 36a).[102] This reaction is thermodynamically favorable, probably because an extended conjugated system is formed. However, the low solubility of the starting compound in all common solvents means that it is impossible to investigate the reaction in solution. After deposition of TAPP on a Cu(111) surface under UHV conditions and annealing at 150 °C, porous networks were formed in which the organic dye molecules are coordinated to Cu atoms through the lone pairs of electrons

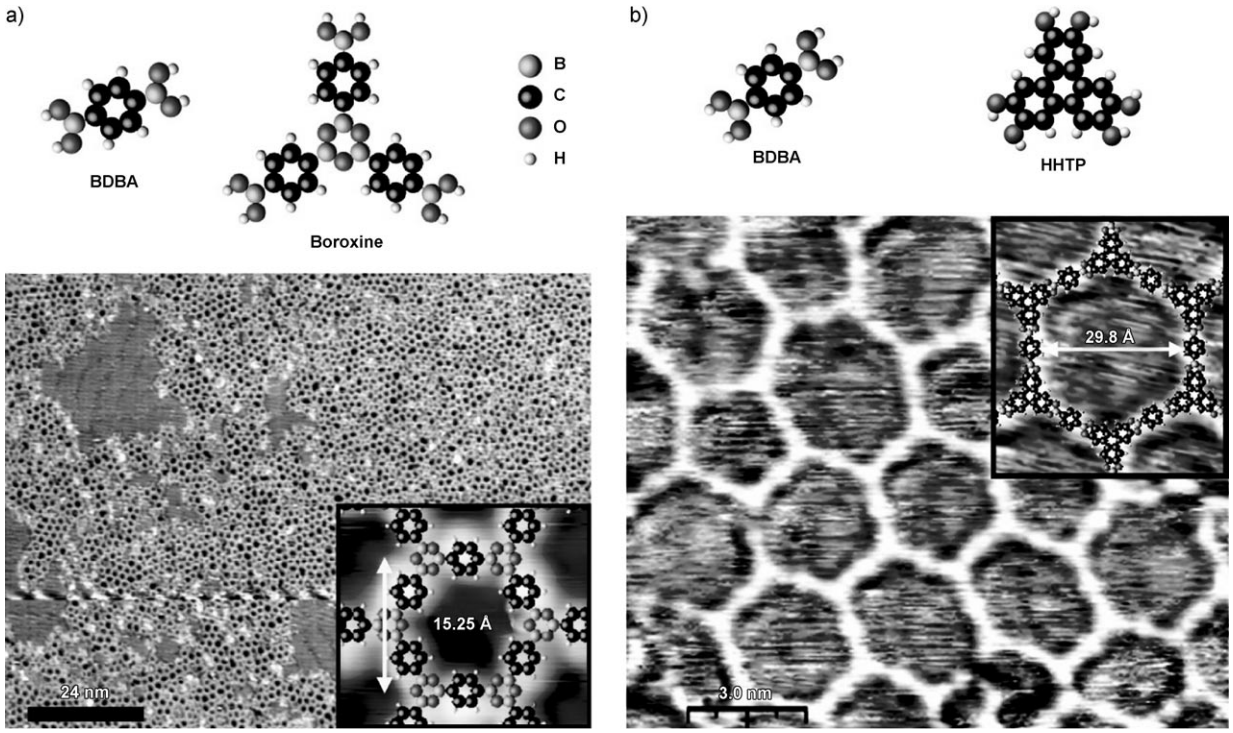

Figure 35. a) Dehydration reaction of BDBA at a Ag(111) surface; top: structure of the reactants; bottom: STM image; b) esterification of BDBA with HHTP at a Ag(111) surface; top: structure of the reactants; bottom: STM image. Insets: molecular models of the networks superimposed on the network structures. Reprinted from Ref. [100] with permission from the American Chemical Society.

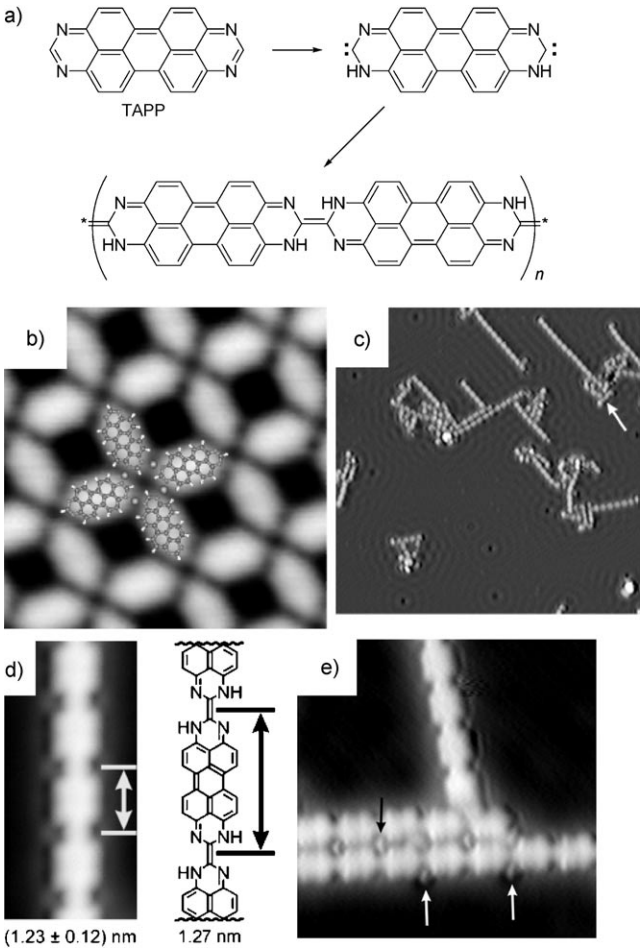

Figure 36. a) Oligomerization of TAPP via a carbene tautomer; b) STM image (5.3×5.3 nm^2) of a network of TAPP on a Cu(111) surface under UHV conditions; the proposed organization of the molecules and their coordination to Cu atoms is highlighted; c) STM image (50×50 nm^2) of polymerized TAPP chains, white arrows point to nucleation sites; d) left: high-resolution STM image (2.4×5 nm^2) of a chain; right: structure of the chain; e) STM image (8×8 nm^2) of a double-stranded band of polymeric TAPP chains, showing the protrusions which are interpreted as Cu atoms (arrows). Reprinted from Ref. [101].)

on their nitrogen atoms (Figure 36b). Further annealing at 250 °C resulted in the formation of oligomeric and polymeric chains which could easily be identified in low-temperature STM images (Figure 36c,d). The covalent linkage of the chains was further confirmed by the fact that it was possible to mechanically manipulate whole chain sections with the STM tip. Interestingly, when two chains were aligned in a parallel fashion, protrusions between them were observed which were interpreted as Cu atoms coordinating to the nitrogen atoms of the oligomers (Figure 36e).

In another example of a coupling reaction, the intermediates have a radical character. Upon thermal activation, a series of *meso*-(*p*-bromophenyl)-substituted porphyrins on a Au(111) substrate under UHV conditions dissociated, whereby the bromine–carbon bonds were cleaved to yield radical species that are prone to dimerization.[103] Depending on the number of reactive substituents on the porphyrin, the formation of dimers, linear arrays, or networks could be controlled (Figure 37). Porphyrins lacking the bromophenyl groups were not reactive. The covalent character of the connectivity was confirmed both by scanning tunneling spectroscopy (STS) experiments and by the fact that lateral manipulation of connected chains by the STM tip was possible, while aggregates that interacted only through van der Waals interactions were broken up.

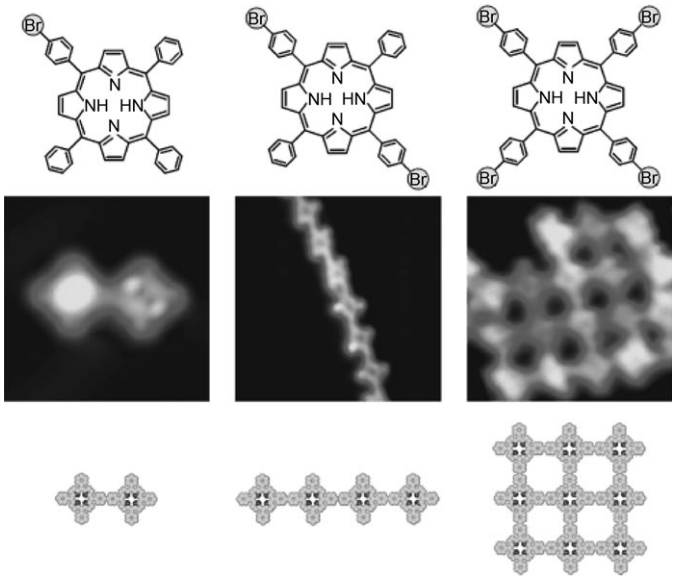

Figure 37. Formation of dimers, linear arrays, and networks by various bromophenyl-substituted porphyrins at a Au(111) surface under UHV conditions. From top to bottom: molecular structures, STM image, and molecular model of the observed structures. Reprinted from Ref. [102] with permission from the Nature Publishing Group.

In related studies, tetrakis(*meso*-mesityl)porphyrins were covalently coupled on a Cu(110) surface under UHV conditions.[104] While these molecules appeared as monomers at room temperature under UHV conditions, annealing between 150 and 200 °C led to their connection into oligomeric structures. STM images revealed that this coupling had taken place through the *meso*-mesityl functions and a mechanism was proposed involving a reduction of their methyl groups to generate CH_2 radicals, which are subsequently coupled to give ethylene linkers,. This covalent coupling mechanism was confirmed by the fact that similar treatment of tetrakis(*meso*-phenyl)porphyrins yielded no coupled products.

Chemical reactivity can also be induced by self-assembly. Dimethyldisulfide molecules were found to self-assemble in linear chains on a Au(100) surface under UHV conditions (Figure 38).[105] Upon the injection of low-energy electrons by a voltage pulse with the STM tip on the terminating molecule of a self-assembled chain, first the sulfur–sulfur bond of that molecule breaks and subsequently a propagating reaction along the molecular chain occurs, and involves a repeated making and breaking of S–S bonds.

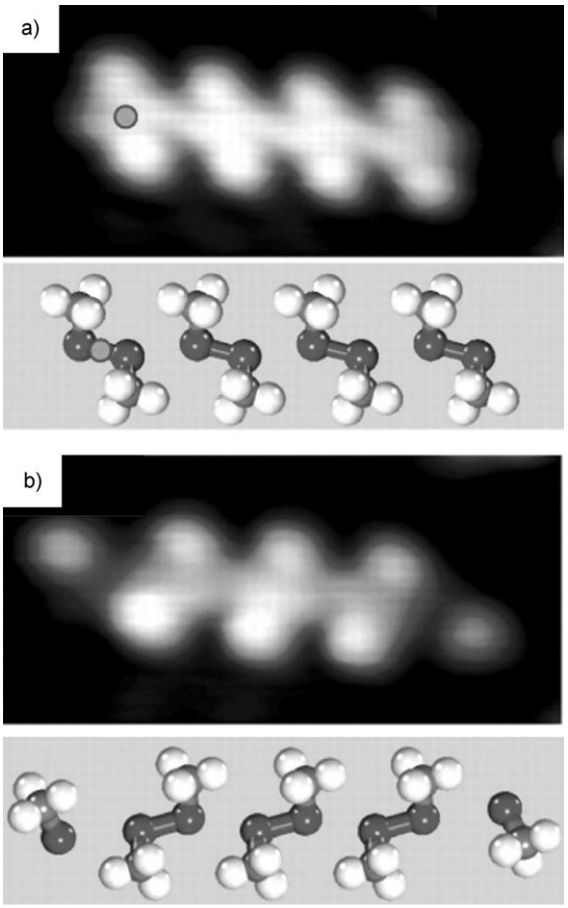

Figure 38. a) STM image (top) and molecular model (bottom) of a chain of four dimethyldisulfide molecules on a Au(100) surface under UHV conditions; the location of the voltage pulse on top of the chain is indicated in the STM images by a dot; b) STM image (top) and molecular model (bottom) of the same location after the chain reaction. Reprinted from Ref. [104] with permission from the American Association for the Advancement of Science.

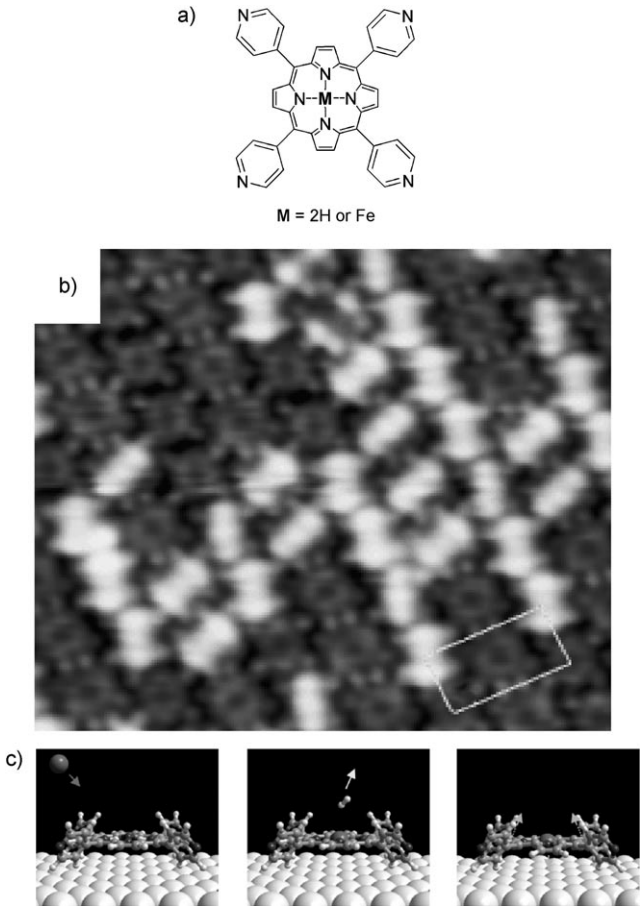

Figure 39. a) Molecular structure of the tetrapyridylporphyrins; b) STM image of a monolayer of porphyrin molecules after exposure to a beam of Fe atoms; the bright rodlike features represent the metalated species; white box: unit cell; c) proposed reaction; left: an Fe atom approaches the porphyrin (see arrow); middle: the two central porphyrin protons are reduced to a molecule of H_2 which dissociates (see arrow), while the Fe atom is oxidized to Fe^{II} and is inserted in the porphyrin; right: Fe porphyrin product, which has adopted a saddle-shape at the surface (see arrow). Reprinted from Ref. [105].

Redox reactions have also been observed in a UHV STM. Auwärter et al. described the controlled metalation of free-base tetrapyridylporphyrins adsorbed on a Ag(111) surface.[106] When a monolayer of these molecules was exposed to Fe atoms provided by an atomic beam, their molecular signature in the STM images changed drastically, while the molecular packing remained the same (Figure 39). In comparison to their original appearance, the new species gave much brighter images and in addition exhibited a reduced symmetry, namely, they appeared rodlike. A possible explanation for this appearance is that the porphyrin molecule adopts a saddlelike conformation, and thereby exhibits a twofold symmetry upon binding of the Fe center. The proposed mechanism of the reaction is shown in Figure 39c, and involves a redox process in which the two protons of the porphyrin are reduced to generate a molecule of H_2, while the Fe atoms are simultaneously oxidized to Fe^{II} upon their inclusion in the porphyrin core.

5.2. Reactivity at Liquid–Solid Interfaces

All of the above-described reactions have in common that they are carried out under rather extreme conditions, such as under ultrahigh vacuum, high pressure, or ultralow temperature. Such conditions are, however, far removed from environments in which most laboratory reactions and biological processes take place, that is, under ambient conditions or in a liquid. So far, only limited studies have been devoted to investigating chemical reactions under ambient conditions by STM. Some examples of simple metal–ligand coordination reactions at a liquid–solid interface have been described, in which a monolayer of bipyridine ligands was first constructed, and then a metal salt was added to the liquid phase.[107] In these cases it is important to note that the metal–ligand coordination reaction does not necessarily take place on the substrate, but more likely in the solution phase where the reaction product accumulates and eventually replaces unreacted ligands at the interface. This is in contrast with

pioneering work in the late 1990s involving the topochemical polymerization of diacetylene compounds at the air–solid and liquid–solid interface, a reaction which was first carried out under UHV conditions[108] but later also in dry monolayers at the graphite–air interface. The STM tip or an external stimulus such as light[109] was used to initiate the polymerization reaction. This approach relies strongly on a careful preorganization of the monomers at the interface, with their reactive groups positioned in proximity and in the desired orientation. In a related study, cinnamate derivatives physisorbed on HOPG were subjected to a light-induced [2+2] photodimerization, which resulted in a change in monolayer structure and tunneling contrast.[110]

More recently, a polymerization at the liquid–solid interface was also described, namely, that of aniline at the interface of Au(111) and an aqueous 0.1 M H_2SO_4 solution in an EC-STM (Figure 40).[111] Increasing the potential of a surface with

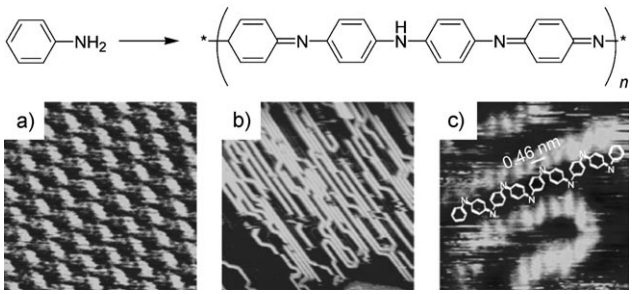

Figure 40. EC-STM images of the electrochemical polymerization of aniline at the interface of Au(111) and an aqueous 0.1 M H_2SO_4 solution; a) monolayer of aniline molecules at 0.9 V; 7×7 nm^2; b) as (a), after raising the potential to 1.05 V; 50×50 nm^2; c) magnification showing the submolecular structure within the polymer chains with aniline monomers arranged in a zigzag fashion; 6×6 nm^2. Reprinted from Ref. [110] with permission from the American Chemical Society.

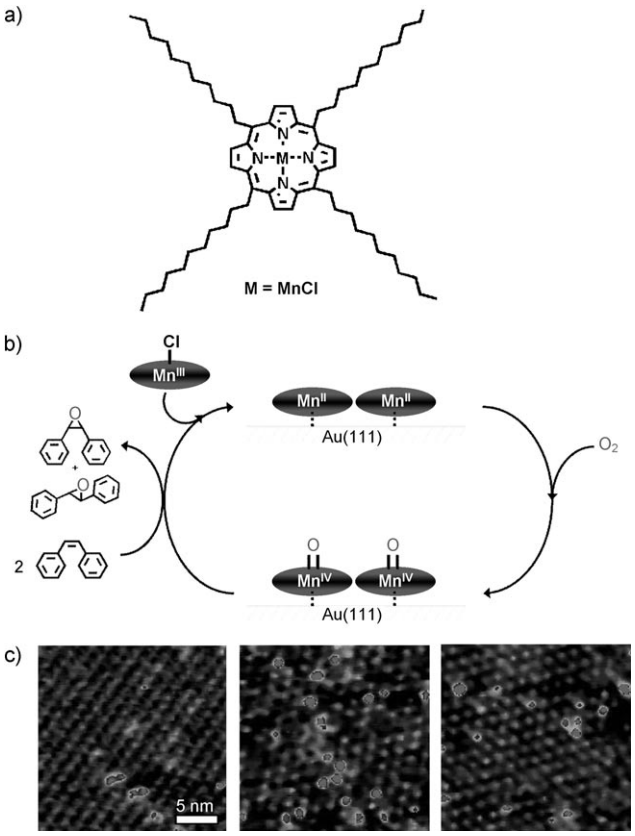

Figure 41. a) Molecular structure of the manganese porphyrin catalyst; b) proposed catalytic cycle; c) series of liquid-cell STM images of a monolayer of the catalysts self-assembled at the interface of Au(111) and *n*-tetradecane; left: system under argon; middle: 4 h after flushing the bell jar with O_2, which causes ca. 10% of the catalyst molecules to be oxidized (bright spots); right: 3 h after the addition of *cis*-stilbene, which shows a decrease in the number of oxidized catalyst molecules.

a monolayer of aniline molecules from 0.9 to 1.05 V induced an oxidative polymerization, which caused the formation of linear polyaniline chains consisting of approximately 100 monomers and with lengths up to 50 nm. The polymerization process appeared to be strongly anisotropic, since a distinct preferential and unprecedented alignment of the polyaniline chains in the [121] direction of the Au(111) surface was observed. Magnifications of the lines revealed their internal structure, with a zigzag ordering of head-to-tail-connected repeating units within the polymer chains.

In a completely different approach, neither the reactants or products of a chemical reaction were imaged by STM, but instead the catalysts of an oxidation reaction were adsorbed at the liquid–solid interface and changes in their topography during a multistep oxidation reaction were followed in real-time.[112] Manganese(III) porphyrins adsorbed at the interface of *n*-tetradecane and Au(111) were found to undergo a reaction upon exposure to molecular oxygen, as was apparent from a threefold increase in the apparent height at the center of the catalyst (Figure 41). Statistical studies revealed that there was a preference for reactions occurring with two adjacent catalysts, which led to the suggestion that each molecule of O_2 had dissociated in a homolytic fashion, thereby distributing its two oxygen atoms over neighboring catalysts. This reaction, which does not occur in solution, was proposed to be activated by the surface through an initial reduction of the manganese centers from Mn^{III} to Mn^{II} upon their adsorption. Both this reduction and the subsequent oxidation to generate $Mn^{IV}=O$ species (Figure 41 b) were confirmed by in situ UV/Vis reflectance measurements.

The $Mn^{IV}=O$ species are active catalysts in the epoxidation of alkenes, and the addition of *cis*-stilbene to the liquid layer resulted in a strong decrease in the number of oxidized catalysts (Figure 41 c). This observation suggested reaction with the alkene, which was confirmed by gas-chromatographic analysis of the liquid layer, which indeed contained the *cis*-stilbene epoxide product.

6. Conclusions and Perspectives

Since the invention of the scanning tunneling microscope, research on supramolecular self-assembly on atomically flat conductive surfaces has witnessed a spectacular increase in activity. By exploiting the concepts from supramolecular chemistry, it is now possible to construct more and more

complex two-dimensional architectures, although, we must admit, serendipity still plays an important role. Despite the confinement of molecules in one plane, which should simplify supramolecular self-assembly, the substrate plays an important role and can in some cases overrule or at least compete with intermolecular interactions.

Supramolecular self-assembly to give chiral architectures highlights important aspects of the subtle interplay between molecules on the one hand and molecules and substrates on the other hand, and has uncovered some of the basic mechanisms of (chiral) molecular recognition, especially under UHV conditions. Key points of interest will remain the investigation of how spontaneous resolution can be achieved, controlled, or templated. Amplification of chirality effects at the liquid–solid interface are also waiting to be explored. For chiral systems, the role of the solvent has barely been touched upon. Such studies will not only reveal solvent-induced chiral expression of molecules on surfaces—in general, important new insights are to be expected regarding the overall role of solvent in directing solvent-assisted supramolecular self-assembly processes on surfaces.

A development in the last five years is the formation of so-called "nanoporous" networks. Primarily driven by academic curiosity, the research activities have revealed a number of previously unexplored aspects of monolayer formation such as control of the concentration and surface coverage, self-recognition and self-selection, and the effect of solvents on self-assembly. Research activities targeting the formation of nanoporous structures provide a wealth of insight into the concepts which drive the formation and stabilization of monolayers (molecule–molecule, molecule–substrate, molecule–solvent interactions, etc.). The main aspect though, which makes the field of two-dimensional nanoporous materials "hot", is the broad range of potential applications. Nanopores can host and immobilize a large variety of guest species. The orientation of the guest species can be determined (visualized), followed in real time, or manipulated, thus offering new concepts for data storage. Such nanopores can be chiral, which paves the way for the future enantioselective adsorption of guest molecules. Nanopores could also act as reaction vessels, for example, for the templated synthesis of inorganic and organic nanoparticles.

An exciting development is the in real-space and real-time exploration of chemical reactions at surfaces, where substrates can affect the outcome of the reaction path, and unique surface-confined nanostructures can be constructed in situ. STM offers the possibility of gaining information of dynamic processes at the level of single molecules and in some cases new aspects of reaction mechanisms are revealed which remain hidden when conventional ensemble techniques are used. It is foreseen that in the near future this new field of STM research, which goes beyond just imaging two-dimensional nanostructures at a surface, will attract increased attention not only from physicists but also from chemists and biologists.

A steadily growing number of scientists appreciate the opportunities which supramolecular self-assembly at surfaces bring, a trend which promises a bright future for this research field, and an area where chemists and physicists meet.

We thank the Interuniversity Attraction Pole program of the Belgian Federal Science Policy Office (PAI 6/27) and K. U. Leuven (GOA). J.A.A.W.E. thanks the Fund of Scientific Research—Flanders (FWO) and K. U. Leuven for financial support.

Received: December 27, 2008
Revised: April 30, 2009

[1] J.-M. Lehn, *Supramolecular Chemistry*, VCH, Weinheim, **1995**.
[2] G. Binning, H. Rohrer, C. Gerber, E. Weibel, *Phys. Rev. Lett.* **1982**, *49*, 57.
[3] a) J. V. Barth, G. Costantini, K. Kern, *Nature* **2005**, *437*, 671; b) M. Ruben, *Angew. Chem.* **2005**, *117*, 1620; *Angew. Chem. Int. Ed.* **2005**, *44*, 1594; c) J. A. A. W. Elemans, S. De Feyter, *Soft Matter* **2009**, *5*, 721.
[4] S. Furukawa, S. De Feyter, *Top. Curr. Chem.* **2009**, *287*, 87.
[5] M. Lackinger, S. Griessl, T. Markert, F. Jamitzky, W. M. Heckl, *J. Phys. Chem. B* **2004**, *108*, 13652.
[6] a) S. Griessl, M. Lackinger, M. Edelwirth, M. Hietschold, W. M. Heckl, *Single Mol.* **2002**, *3*, 25; b) N. Dmitriev, N. Lin, J. Weckesser, J. V. Barth, K. Kern, *J. Phys. Chem. B* **2002**, *106*, 6907.
[7] T. Kudernac, S. Lei, J. A. A. W. Elemans, S. De Feyter, *Chem. Soc. Rev.* **2009**, *38*, 402.
[8] S. J. H. Griessl, M. Lackinger, F. Jamitzky, T. Markert, M. Hietschold, W. M. Heckl, *J. Phys. Chem. B* **2004**, *108*, 11556.
[9] S. J. H. Griessl, M. Lackinger, F. Jamitzky, T. Markert, M. Hietschold, W. M. Heckl, *Langmuir* **2004**, *20*, 9403.
[10] a) S. De Feyter, A. Gesquière, M. Klapper, K. Müllen, F. C. De Schryver, *Nano Lett.* **2003**, *3*, 1485; b) K. G. Nath, O. Ivasenko, J. A. Miwa, H. Dang, J. D. Wuest, A. Nanci, D. F. Perepichka, F. Rosei, *J. Am. Chem. Soc.* **2006**, *128*, 4212.
[11] M. O. Blunt, J. C. Russell, M. del Carmen Giménez-López, J. P. Garrahan, X. Lin, M. Schröder, N. L. Champness, P. H. Beton, *Science* **2008**, *322*, 1077.
[12] a) J. A. A. W. Elemans, M. C. Lensen, J. W. Gerritsen, H. van Kempen, S. Speller, R. J. M. Nolte, A. E. Rowan, *Adv. Mater.* **2003**, *15*, 2070; b) M. C. Lensen, S. J. T. van Dingenen, J. A. A. W. Elemans, H. P. Dijkstra, G. P. M. van Klink, G. van Koten, J. W. Gerritsen, S. Speller, R. J. M. Nolte, A. E. Rowan, *Chem. Commun.* **2004**, 762; c) M. C. Lensen, J. A. A. W. Elemans, S. J. T. van Dingenen, J. W. Gerritsen, S. Speller, A. E. Rowan, R. J. M. Nolte, *Chem. Eur. J.* **2007**, *13*, 7948; d) M. Surin, P. Samorì, A. Jouaiti, N. Kyritsakas, M. W. Hosseini, *Angew. Chem.* **2007**, *119*, 249; *Angew. Chem. Int. Ed.* **2007**, *46*, 245.
[13] a) M. S. Alam, S. Strömsdörfer, V. Dremov, P. Müller, J. Kortus, M. Ruben, J.-M. Lehn, *Angew. Chem.* **2005**, *117*, 8109; *Angew. Chem. Int. Ed.* **2005**, *44*, 7896; b) A. Semenov, J. P. Spatz, M. Möller, J.-M. Lehn, B. Sell, D. Schubert, C. H. Weidl, U. S. Schubert, *Angew. Chem.* **1999**, *111*, 2701; *Angew. Chem. Int. Ed.* **1999**, *38*, 2547; c) A. Mourran, U. Ziener, M. Möller, E. Breuning, M. Ohkita, J.-M. Lehn, *Eur. J. Inorg. Chem.* **2005**, 2641.
[14] A. Langner, S. L. Tait, N. Lin, C. Rajadurai, M. Ruben, K. Kern, *Proc. Natl. Acad. Sci. USA* **2007**, *104*, 17927.
[15] S. Berner, M. de Wild, L. Ramoino, S. Ivan, A. Baratoff, H.-J. Günterodt, H. Suzuki, D. Schlettwein, T. A. Jung, *Phys. Rev. B* **2003**, *68*, 115410.
[16] M. de Wild, S. Berner, H. Suzuki, H. Yanagi, D. Schlettwein, S. Ivan, A. Baratoff, H.-J. Günterodt, T. A. Jung, *ChemPhysChem* **2002**, *3*, 881.
[17] a) F. Klappenberger, M. E. Cañas-Ventura, S. Clair, S. Pons, U. Schlickum, Z.-R. Qu, H. Brune, K. Kern, T. Strunskus, C. Wöll,

A. Comisso, A. De Vita, M. Ruben, J. V. Barth, *ChemPhysChem* **2007**, *8*, 1782; b) F. Klappenberger, M. E. Cañas-Ventura, S. Clair, S. Pons, U. Schlickum, Z.-R. Qu, T. Strunskus, A. Comisso, C. Wöll, H. Brune, K. Kern, A. De Vita, M. Ruben, J. V. Barth, *ChemPhysChem* **2008**, *9*, 2522.
[18] S. Cincotti, J. P. Rabe, *Appl. Phys. Lett.* **1993**, *62*, 3531.
[19] L. Nony, E. Gnecco, A. Baratoff, A. Alkauskas, R. Bennewitz, O. Pfeiffer, S. Maier, A. Wetzel, E. Meyer, C. Gerber, *Nano Lett.* **2004**, *4*, 2185.
[20] L. Ramoino, M. von Arx, S. Schintke, A. Baratoff, H.-J. Günterodt, T. A. Jung, *Chem. Phys. Lett.* **2006**, *417*, 22.
[21] S. Maier, L. Fendt, L. Zimmerli, T. Glatzel, O. Pfeiffer. F. Diederich, E. Meyer, *Small* **2008**, *4*, 1115.
[22] J. P. Rabe and S. Buchholz, *Science* **1991**, *253*, 424.
[23] H. J. Räder, A. Rouhanipour, A. M. Talarico, V. Palermo, P. Samorì, K. Müllen, *Nat. Mater.* **2006**, *5*, 276.
[24] F. Trixler, T. Markert, M. Lackinger, F. Jamitzky, W. M. Heckl, *Chem. Eur. J.* **2007**, *13*, 7785.
[25] L. Pasteur, *Ann. Chim. Phys.* **1848**, *24*, 442.
[26] a) S. M. Barlow, R. Raval, *Surf. Sci. Rep.* **2003**, *50*, 201; b) N. Katsonis, E. Lacaze, B. L. Feringa, *J. Mater. Chem.* **2008**, *18*, 2065; c) K.-H. Ernst, *Top. Curr. Chem.* **2006**, *265*, 209; d) S. M. Barlow, R. Raval, *Curr. Opin. Colloid Interface Sci.* **2008**, *13*, 65; e) K.-H. Ernst, *Curr. Opin. Colloid Interface Sci.* **2008**, *13*, 54; f) L. Pérez-García, D. B. Amabilino, *Chem. Soc. Rev.* **2007**, *36*, 941; g) J. A. A. W. Elemans, I. De Cat, H. Xu, S. De Feyter, *Chem. Soc. Rev.* **2009**, *38*, 402.
[27] a) F. Stevens, D. J. Dyer, D. M. Walba, *Angew. Chem.* **1996**, *108*, 955; *Angew. Chem. Int. Ed. Engl.* **1996**, *35*, 900; b) S. De Feyter, P. C. M. Grim, M. Rücker, P. Vanoppen, C. Meiners, M. Sieffert, S. Valiyaveettil, K. Müllen, F. C. De Schryver, *Angew. Chem.* **1998**, *110*, 1281; *Angew. Chem. Int. Ed.* **1998**, *37*, 1223.
[28] K. E. Plass, A. L. Grzesiak, A. J. Matzger, *Acc. Chem. Res.* **2007**, *40*, 287.
[29] A. Kühnle, T. R. Linderoth, B. Hammer, F. Besenbacher, *Nature* **2002**, *415*, 891.
[30] M. Böhringer, K. Morgenstern, W.-D. Schneider, R. Berndt, F. Mauri, A. De Vita, R. Car, *Phys. Rev. Lett.* **1999**, *83*, 324.
[31] M. Ortega Lorenzo, C. J. Baddeley, C. Muryn, R. Raval, *Nature* **2000**, *404*, 376.
[32] a) M. Linares, P. Iavicoli, K. Psychogyiopoulou, D. Beljonne, S. De Feyter, R. Lazzaroni, D. B. Amabilino, *Langmuir* **2008**, *24*, 9566; b) J. Zhang, A. Gesquière, M. Sieffert, M. Klapper, K. Müllen, F. C. De Schryver, S. De Feyter, *Nano Lett.* **2005**, *5*, 1395.
[33] M. Lingenfelder, G. Tomba, G. Costantini, L. Colombi Ciacchi, A. De Vita, K. Kern, *Angew. Chem.* **2007**, *119*, 4576; *Angew. Chem. Int. Ed.* **2007**, *46*, 4492.
[34] a) J. Weckesser, A. De Vita, J. V. Barth, C. Cai, K. Kern, *Phys. Rev. Lett.* **2001**, *87*, 096101; b) C. B. France, B. Parkinson, *J. Am. Chem. Soc.* **2003**, *125*, 12712.
[35] J. V. Barth, J. Weckesser, G. Trimarchi, M. Vladimirova, A. De Vita, C. Cai, H. Brune, P. Günter, K. Kern, *J. Am. Chem. Soc.* **2002**, *124*, 7991.
[36] a) F. Tao, S. L. Bernasek, *J. Phys. Chem. B* **2005**, *109*, 6233; b) L. Merz, H. Güntherodt, L. J. Scherer, E. C. Constable, C. E. Housecroft, M. Neuburger, B. A. Herrmann, *Chem. Eur. J.* **2005**, *11*, 2307.
[37] N. Lin, S. Stepanow, F. Vidal, K. Kern, M. S. Alam, S. Strömsdörfer, V. Dremov, P. Müller, A. Landa, M. Ruben, *Dalton Trans.* **2006**, 2794.
[38] S. Weigelt, C. Busse, L. Petersen, E. Rauls, B. Hammer, K. V. Gothelf, F. Besenbacher, T. R. Linderoth, *Nat. Mater.* **2006**, *5*, 112.
[39] Q. Chen, N. Richardson, *Nat. Mater.* **2003**, *2*, 324.
[40] a) S. De Feyter, A. Gesquière, K. Wurst, D. B. Amabilino, J. Veciana, F. C. De Schryver, *Angew. Chem.* **2001**, *113*, 3317; *Angew. Chem. Int. Ed.* **2001**, *40*, 3217; b) W. Mamdouh, H. Uji-i, A. Gesquière, S. De Feyter, D. B. Amabilino, M. M. S. Abdel-Mottaleb, J. Veciana, F. C. De Schryver, *Langmuir* **2004**, *20*, 9628.
[41] Y. Wei, K. Kannappan, G. W. Flynn, M. B. Zimmt, *J. Am. Chem. Soc.* **2004**, *126*, 5318.
[42] a) V. Humblot, M. O. Lorenzo, C. J. Baddeley, S. Haq, R. Raval, *J. Am. Chem. Soc.* **2004**, *126*, 6460; b) N. Liu, S. Haq, G. R. Darling, R. Raval, *Angew. Chem.* **2007**, *119*, 7757; *Angew. Chem. Int. Ed.* **2007**, *46*, 7613.
[43] R. Fasel, M. Parschau, K.-H. Ernst, *Angew. Chem.* **2003**, *115*, 5336; *Angew. Chem. Int. Ed.* **2003**, *42*, 5178.
[44] R. Fasel, M. Parschau, K. H. Ernst, *Nature* **2006**, *439*, 449.
[45] N. Katsonis, H. Xu, R. M. Haak, T. Kudernac, Z. Tomović, S. George, M. Van der Auweraer, A. P. H. J. Schenning, E. W. Meijer, B. L. Feringa, S. De Feyter, *Angew. Chem.* **2008**, *120*, 5075; *Angew. Chem. Int. Ed.* **2008**, *47*, 4997.
[46] a) J. D. Mougous, A. J. Brackley, K. Foland, R. T. Baker, D. L. Patrick, *Phys. Rev. Lett.* **2000**, *84*, 2742; b) A. M. Berg, D. L. Patrick, *Angew. Chem.* **2005**, *117*, 1855; *Angew. Chem. Int. Ed.* **2005**, *44*, 1821.
[47] F. Cicoira F, C. Santato, F. Rosei, *Top. Curr. Chem.* **2008**, *285*, 203.
[48] Y. Ye, W. Sun, Y. Wang, X. Shao, X. Xu, F. Cheng, J. Li, K. Wu, *J. Phys. Chem. C* **2007**, *111*, 10138.
[49] M. Lackinger, S. Griessl, W. M. Heckl, M. Hietschold, G. W. Flynn, *Langmuir* **2005**, *21*, 4984.
[50] M. Ruben, D. Payer, A. Landa, A. Comisso, C. Gattinoni, N. Lin, J. P. Collin, J. P. Sauvage, A. De Vita, K. Kern, *J. Am. Chem. Soc.* **2006**, *128*, 15644.
[51] L. Kampschulte, M. Lackinger, A. K. Maier, R. S. K. Kishore, S. Griessl, M. Schmittel, W. M. Heckl, *J. Phys. Chem. B* **2006**, *110*, 10829.
[52] J. Lu, S. Lei, Q. Zeng, S. Kang, C. Wang, L. Wan, C. Bai, *J. Phys. Chem. B* **2004**, *108*, 5161.
[53] a) H. Zhou, H. Dang, J. H. Yi, A. Nanci, A. Rochefort, J. D. Wuest, *J. Am. Chem. Soc.* **2007**, *129*, 13774; b) M. Blunt, X. Lin, M. D. Gimenez-Lopez, M. Schröder, N. R. Champness, P. H. Beton, *Chem. Commun.* **2008**, 2304.
[54] U. Schlickum, R. Decker, F. Klappenberger, G. Zoppellaro, S. Klyatskaya, W. Auwärter, S. Neppl, K. Kern, H. Brune, M. Ruben, J. V. Barth, *J. Am. Chem. Soc.* **2008**, *130*, 11778.
[55] G. Pawin, K. L. Wong, K.-Y. Kwon, L. Bartels, *Science* **2006**, *313*, 961.
[56] J. A. Theobald, N. S. Oxtoby, M. A. Philips, N. R. Champness, P. H. Beton, *Nature* **2003**, *424*, 1029.
[57] a) A. Dmitriev, H. Spillmann, N. Lin, J. V. Barth, K. Kern, *Angew. Chem.* **2003**, *115*, 2774; *Angew. Chem. Int. Ed.* **2003**, *42*, 2670; b) S. Stepanow, M. Lingenfelder, A. Dmitriev, H. Spillmann, E. Delvigne, N. Lin, X. Deng, C. Cai, J. V. Barth, K. Kern, *Nat. Mater.* **2004**, *3*, 229.
[58] S. Stepanow, N. Lin, D. Payer, U. Schlickum, F. Klappenberger, G. Zoppellaro, M. Ruben, H. Brune, J. V. Barth, K. Kern, *Angew. Chem.* **2007**, *119*, 724; *Angew. Chem. Int. Ed.* **2007**, *46*, 710.
[59] S. L. Tait, A. Langner, N. Lin, R. Chandrasekar, O. Fuhr, M. Ruben, *ChemPhysChem* **2008**, *9*, 2495.
[60] A. Cnossen, D. Pijper, T. Kudernac, M. M. Pollard, N. Katsonis, B. L. Feringa, *Chem. Eur. J.* **2009**, *15*, 2768.
[61] S. Furukawa, H. Uji-i, K. Tahara, T. Ichikawa, M. Sonoda, F. C. De Schryver, Y. Tobe and S. De Feyter, *J. Am. Chem. Soc.* **2006**, *128*, 3502.
[62] K. Tahara, C. A. Johnson II, T. Fujita, M. Sonoda, F. C. De Schryver, S. De Feyter, M. M. Haley, Y. Tobe, *Langmuir* **2007**, *23*, 10190.
[63] a) G. Schull, L. Douillard, C. Fiorini-Debuisschert, F. Charra, F. Mathevet, D. Kreher, A. J. Attias, *Nano Lett.* **2006**, *6*, 1360;

b) G. Schull, L. Douillard, C. Fiorini-Debuisschert, F. Charra, F. Mathevet, D. Kreher, A. J. Attias, *Adv. Mater.* **2006**, *18*, 2954.
[64] Z. Ma, Y. Wang, P. Wang, W. Huang, Y. Li, S. B. Lei, Y. L. Yang, X. L. Fan, C. Wang, *ACS Nano* **2007**, *1*, 160.
[65] J. R. Gong, L. J. Wan, Q. H. Yuan, C. L. Bai, H. Jude, P. J. Stang, *Proc. Natl. Acad. Sci. USA* **2005**, *102*, 971.
[66] a) Y. Ye, W. Sun, Y. Wang, X. Shao, X. Xu, F. Cheng, J. Li, K. Wu, *J. Phys. Chem. C* **2007**, *111*, 10138; b) W. Xiao, X. Feng, P. Ruffieux, O. Gröning, K. Müllen, R. Fasel, *J. Am. Chem. Soc.* **2008**, *130*, 8910; c) M. Stöhr, M. Wahl, C. H. Galka, T. Riehm, T. A. Jung, L. H. Gade, *Angew. Chem.* **2005**, *117*, 7560; *Angew. Chem. Int. Ed.* **2005**, *44*, 7394.
[67] K. Tahara, S. Furukawa, H. Uji-i, T. Uchino, T. Ichikawa, J. Zhang, W. Mamdouh, M. Sonoda, F. C. De Schryver, S. De Feyter, Y. Tobe, *J. Am. Chem. Soc.* **2006**, *128*, 16613.
[68] C.-A. Palma, M. Bonini, A. Llanes-Pallas, T. Breiner, M. Prato, D. Bonifazi, P. Samorì, *Chem. Commun.* **2008**, 5289.
[69] S. Lei, K. Tahara, F. C. De Schryver, M. Van der Auweraer, Y. Tobe, S. De Feyter, *Angew. Chem.* **2008**, *120*, 3006; *Angew. Chem. Int. Ed.* **2008**, *47*, 2964.
[70] a) L. Kampschulte, T. L. Werblowsky, R. S. K. Kishore, M. Schmittel, W. M. Heckl, M. Lackinger, *J. Am. Chem. Soc.* **2008**, *130*, 8502; b) C. A. Palma, M. Bonini, A. Llanes-Pallas, T. Breiner, M. Prato, D. Bonifazi, P. Samorì, *Chem. Commun.* **2008**, 5289.
[71] U. Schlickum, R. Decker, F. Klappenberger, G. Zoppellaro, S. Klyatskaya, M. Ruben, I. Silanes, A. Arnau, K. Kern, H. Brune, J. V. Barth, *Nano Lett.* **2007**, *7*, 3813.
[72] K. Tahara, S. Lei, D. Mössinger, H. Kozuma, K. Inukai, M. Van der Auweraer, F. C. De Schryver, S. Höger, Y. Tobe, S. De Feyter, *Chem. Commun.* **2008**, 3897.
[73] N. Wintjes, J. Hornung, J. Lobo-Checa, T. Voigt, T. Samuely, C. Thilgen, M. Stöhr, F. Diederich, T. A. Jung, *Chem. Eur. J.* **2008**, *14*, 5794.
[74] S. J. H. Griessl, M. Lackinger, F. Jamitzky, T. Markert, M. Hietschold, W. M. Heckl, *J. Phys. Chem. B* **2004**, *108*, 11556.
[75] A. Kiebele, D. Bonifazi, F. Cheng, M. Stöhr, F. Diederich, T. Jung, H. Spillmann, *ChemPhysChem* **2006**, *7*, 1462.
[76] S. Lei, M. Surin, K. Tahara, J. Adisoejoso, R. Lazzaroni, Y. Tobe, S. De Feyter, *Nano Lett.* **2008**, *8*, 2541.
[77] M. Li, K. Deng, S. B. Lei, Y. L. Yang, T. S. Wang, Y. T. Shen, C. R. Wang, Q. D. Zeng, C. Wang, *Angew. Chem.* **2008**, *120*, 6819; *Angew. Chem. Int. Ed.* **2008**, *47*, 6717.
[78] M. Stöhr, M. Wahl, H. Spillmann, L. H. Gade, T. A. Jung, *Small* **2007**, *3*, 1336.
[79] N. Wintjes, D. Bonifazi, F. Cheng, A. Kiebele, M. Stöhr, T. Jung, H. Spillmann, F. Diederich, *Angew. Chem.* **2007**, *119*, 4167; *Angew. Chem. Int. Ed.* **2007**, *46*, 4089.
[80] M. Wahl, M. Stöhr, H. Spillmann, T. A. Jung, L. H. Gade, *Chem. Commun.* **2007**, 1349.
[81] L. M. A. Perdigão, A. Saywell, G. N. Fontes, P. A. Staniec, G. Goretzki, A. G. Phillips, N. R. Champness, P. H. Beton, *Chem. Eur. J.* **2008**, *14*, 7600.
[82] R. Madueno, M. T. Räisänen, C. Silien, M. Buck, *Nature* **2008**, *454*, 618.
[83] L. Piot, D. Bonifazi, P. Samorì, *Adv. Funct. Mater.* **2007**, *17*, 3689.
[84] a) M. B. J. Roeffaers, B. F. Sels, H. Uji-i, F. C. De Schryver, P. A. Jacobs, D. E. de Vos, J. Hofkens, *Nature* **2006**, *439*, 572; b) M. B. J. Roeffaers, G. De Cremer, H. Uji-i, B. Muls, B. F. Sels, P. A. Jacobs, F. C. De Schryver, D. E. De Vos, J. Hofkens, *Proc. Natl. Acad. Sci. USA* **2007**, *104*, 12603.
[85] a) H. P. Lu, L. Xu, X. S. Xie, *Science* **1998**, *282*, 1877; b) K. Velonia, O. Flomenbom, D. Loos, S. Masuo, M. Cotlet, Y. Engelborghs, J. Hofkens, A. E. Rowan, J. Klafter, R. J. M. Nolte, F. C. De Schryver, *Angew. Chem.* **2005**, *117*, 566; *Angew. Chem. Int. Ed.* **2005**, *44*, 560; c) O. Flomenbom, K. Velonia, D. Loos, S. Masuo, M. Cotlet, Y. Engelborghs, J. Hofkens, A. E. Rowan, R. J. M. Nolte, F. C. De Schryver, J. Klafter, *Proc. Natl. Acad. Sci. USA* **2005**, *102*, 2368; d) N. S. Hatzakis, H. Engelkamp, K. Velonia, J. Hofkens, P. C. M. Christianen, A. Svendsen, S. A. Patkar, J. Vind, J. C. Maan, A. E. Rowan, R. J. M. Nolte, *Chem. Commun.* **2006**, 2012; e) V. Martínez Martínez, G. De Cremer, M. B. J. Roeffaers, M. Sliwa, M. Baruah, D. E. De Vos, J. Hofkens, B. F. Sels, *J. Am. Chem. Soc.* **2008**, *130*, 13192.
[86] W. Xu, J. S. Kong, Y.-T. E. Yeh, P. Chen, *Nat. Mater.* **2008**, *7*, 992.
[87] A. Kiel, J. Kovacs, A. Mokhir, R. Krämer, D.-P. Herten, *Angew. Chem.* **2007**, *119*, 3427; *Angew. Chem. Int. Ed.* **2007**, *46*, 3363.
[88] a) B. J. McIntyre, M. B. Salmeron, G. A. Somorjai, *Catal. Lett.* **1992**, *14*, 263; b) L. Ruan, F. Besenbacher, I. Stensgaard, E. Lægsgaard, *Phys. Rev. Lett.* **1992**, *69*, 3523; c) F. M. Leibsle, P. W. Murray, S. M. Francis, G. Thornton, M. Bowker, *Nature* **1993**, *363*, 706.
[89] G. Ertl, *Angew. Chem.* **2008**, *120*, 3578; *Angew. Chem. Int. Ed.* **2008**, *47*, 3524.
[90] a) J. R. Hahn, W. Ho, *Phys. Rev. Lett.* **2001**, *87*, 166102; b) B. L. M. Hendriksen, J. W. Frenken, *Phys. Rev. Lett.* **2002**, *89*, 046101.
[91] B. C. Stipe, M. A. Rezaei, W. Ho, *Phys. Rev. Lett.* **1998**, *81*, 1263.
[92] a) T. Komeda, Y. Kim, M. Kawai, B. N. J. Persson, H. Ueba, *Science* **2002**, *295*, 2055; b) K. Morgenstern, K. H. Rieder, *J. Chem. Phys.* **2002**, *116*, 5746.
[93] a) Y. Kim, T. Komeda, M. Kawai, *Phys. Rev. Lett.* **2002**, *89*, 126104; b) K. Morgenstern, K.-H. Rieder, *Chem. Phys. Lett.* **2002**, *358*, 250.
[94] a) X. H. Qiu, G. V. Nazin, W. Ho, *Phys. Rev. Lett.* **2004**, *93*, 196806; b) J. Henzl, M. Mehlhorn, H. Gawronski, K.-H. Rieder, K. Morgenstern, *Angew. Chem.* **2006**, *118*, 617; *Angew. Chem. Int. Ed.* **2006**, *45*, 603; c) M. J. Comstock, N. Levy, A. Kirakosian, J. Cho, F. Lauterwasser, J. H. Harvey, D. A. Strubbe, J. M. J. Fréchet, D. Trauner, S. G. Louie, M. F. Crommie, *Phys. Rev. Lett.* **2007**, *99*, 038301; d) R. Arai, S. Uemura, M. Irie, K. Matsuda, *J. Am. Chem. Soc.* **2008**, *130*, 9371; e) S. B. Lei, K. Deng, Y. L. Yang, Q. D. Zeng, C. Wang, J. Z. Jiang, *Nano Lett.* **2008**, *8*, 1836.
[95] P. Samorí, C. D. Simpson, K. Müllen, J. P. Rabe, *Langmuir* **2002**, *18*, 4183.
[96] A. Gourdon, *Angew. Chem.* **2008**, *120*, 7056; *Angew. Chem. Int. Ed.* **2008**, *47*, 6950.
[97] S. Weigelt, C. Busse, C. Bombis, M. M. Knudsen, K. V. Gothelf, T. Strunskus, C. Wöll, M. Dahlbom, B. Hammer, E. Lægsgaard, F. Besenbacher, T. R. Linderoth, *Angew. Chem.* **2007**, *119*, 9387; *Angew. Chem. Int. Ed.* **2007**, *46*, 9227.
[98] S. Weigelt, C. Bombis, C. Busse, M. M. Knudsen, K. V. Gothelf, E. Lægsgaard, F. Besenbacher, T. R. Linderoth, *ACS Nano* **2008**, *2*, 651.
[99] S. Weigelt, C. Busse, C. Bombis, M. M. Knudsen, K. V. Gothelf, E. Lægsgaard, F. Besenbacher, T. R. Linderoth, *Angew. Chem.* **2008**, *120*, 4478; *Angew. Chem. Int. Ed.* **2008**, *47*, 4406.
[100] M. Treier, N. V. Richardson, R. Fasel, *J. Am. Chem. Soc.* **2008**, *130*, 14054.
[101] N. A. A. Zwaneveld, R. Pawlak, M. Abel, D. Catalin, D. Gigmes, D. Bertin, L. Porte, *J. Am. Chem. Soc.* **2008**, *130*, 6678.
[102] M. Matena, T. Riehm, M. Stöhr, T. A. Jung, L. H. Gade, *Angew. Chem.* **2008**, *120*, 2448; *Angew. Chem. Int. Ed.* **2008**, *47*, 2414.
[103] L. Grill, M. Dyer, L. Lafferentz, M. Persson, M. V. Peters, S. Hecht, *Nat. Nanotechnol.* **2007**, *2*, 687.
[104] M. In't Veld, P. Iavicoli, S. Haq, D. B. Amabilino, R. Raval, *Chem. Commun.* **2008**, 1536.
[105] P. Maksymovych, D. S. Sorescu, K. D. Jordan, J. T. Yates, Jr., *Science* **2008**, *322*, 1664.

[106] W. Auwärter, A. Weber-Bargioni, S. Brink, A. Riemann, A. Schiffrin, M. Ruben, J. V. Barth, *ChemPhysChem* **2007**, *8*, 250.
[107] a) M. M. S. Abdel-Mottaleb, N. Schuurmans, S. De Feyter, J. van Esch, B. L. Feringa, F. C. De Schryver, *Chem. Commun.* **2002**, 1894; b) Y. Kikkawa, E. Koyama, S. Tsuzuki, K. Fujiwara, K. Miyake, H. Tokuhisa, M. Kanesato, *Langmuir* **2006**, *22*, 6910.
[108] Y. Okawa, M. Aono, *Nature* **2001**, *409*, 683.
[109] P. C. M. Grim, S. De Feyter, A. Gesquière, P. Vanoppen, M. Rücker, S. Valiyaveettil, G. Moessner, K. Müllen, F. C. De Schryver, *Angew. Chem.* **1997**, *109*, 2713; *Angew. Chem. Int. Ed. Engl.* **1997**, *36*, 2601.
[110] M. M. S. Abdel-Mottaleb, S. De Feyter, A. Gesquière, M. Sieffert, M. Klapper, K. Müllen, F. C. De Schryver, *Nano Lett.* **2001**, *1*, 353.
[111] L. Y. O. Yang, C. Chang, S. Liu, C. Wu, S. L. Yau, *J. Am. Chem. Soc.* **2007**, *129*, 8076.
[112] B. Hulsken, R. van Hameren, J. W. Gerritsen, T. Khoury, P. Thordarson, M. J. Crossley, A. E. Rowan, R. J. M. Nolte, J. A. A. W. Elemans, S. Speller, *Nat. Nanotechnol.* **2007**, *2*, 285.
[113] S. W. Hla, L. Bartels, G. Meyer, K.-H. Rieder, *Phys. Rev. Lett.* **2000**, *85*, 2777.

